

In This Issue:



Departments

News Briefs

DEVELOPMENTS	527
NBS, Westinghouse to Calibrate New Radiation Detectors	
Industry, NBS Working to Improve Carpet Fire Test	
Role of Standards in World Trade Reported	
First Measurements of Ultra-Cold Atomic Collisions	
NBS Finds DAT Copy-Prevention System Deficient	
New Telephone Service to Set Clocks in Computers	
Improving Aircraft Safety is Goal of Joint Federal Research Project	
<hr/>	
STANDARD REFERENCE MATERIALS	529
New Samples to Aid in Measuring Cholesterol, Vitamins	
<hr/>	
STANDARD REFERENCE DATA	529
New Diffraction and Crystal Databases Available	
<hr/>	
CALENDAR	530

Articles

An Improvement in the Reliability of Standard Cell Enclosures	Bruce F. Field and Liu Ruimin	533
The NBS Vision System in the AMRF	Marilyn Nashman and Karen J. Chaconas	539
International Comparisons of Pressure Standards: A Status Report	Charles R. Tilford	545
Condensation Method for Humidity Measurement in the UMR Cloud Simulation Chamber	D. E. Hagen, D. R. White, and D. J. Alofs	551
Precipitation of $\text{NH}_4\text{UO}_2\text{PO}_4 \cdot 3\text{H}_2\text{O}$ — Solubility and Structural Comparison with Alkali Uranyl(2+) Phosphates	Milenko Marković, Nevenka Pavković, and Neven D. Pavković	557
Practical Uncertainty Limits to the Mass Determination of a Piston- Gage Weight	R. S. Davis and B. E. Welch	565

News Briefs

Developments

NBS, WESTINGHOUSE TO CALIBRATE NEW RADIATION DETECTORS

NBS and the Westinghouse Research and Development Center are engaged in a cooperative research program to develop techniques to *verify calibrations of a new generation of solid state track recorders (SSTRs) recently introduced by Westinghouse for the nuclear power industry*. SSTRs are passive radiation detectors used in nuclear power reactors to monitor the accumulated neutron radiation dose received by critical components, such as the containment vessel. Because neutrons from the reactor core gradually embrittle steel, this accumulated dose is a major factor in determining the safe operating lifetime of many first-generation power reactors. Calibration of an SSTR requires an accurate measurement of minute masses of uranium, plutonium, and neptunium. The new Westinghouse SSTRs use extremely thin deposits of these fissionable materials—picogram (0.000 000 000 001 g) amounts. Using special fission-rate measurement capabilities and microgram-size mass standards, bureau scientists are helping Westinghouse develop mass assay procedures that enhance the reliability of these detectors.

INDUSTRY, NBS WORKING TO IMPROVE CARPET FIRE TEST

Interior materials such as carpeting can be highly flammable, contributing to the spread of a fire. Several tests are available to determine the flammability of carpets, including one developed by NBS in the 1970s to *estimate flame spread of*

floor coverings in corridors and exitways. In a project funded by the Carpet and Rug Institute, the American Textile Manufacturers Institute, and the Man-Made Fiber Producers Association, the NBS Center for Fire Research is working to *improve this widely used test method*. It was adopted in 1978 as a voluntary industry test method (Critical Radiant Flux of Floor-Covering Systems Using a Radiant Heat Energy Source, ASTM E 648). This project was prompted by some variations in results during a recent round of testing by industry laboratories. NBS will study all factors which might influence the test and recommend changes in the apparatus, test procedure, and/or interpretation of the results. A final report will be issued by NBS in spring 1989.

ROLE OF STANDARDS IN WORLD TRADE REPORTED

NBS recently examined the level of U.S. participation in selected international standardization activities. A preliminary analysis of the data shows *some correlation between U.S. participation and recent export performance for several major product categories*. The report offers recommendations for enhancing U.S. international competitiveness through increased participation in standardization activities. The report also describes the role of international standards, their increasing importance in world trade, and the extent of past and current U.S. participation in the two major international standardization bodies, the International Organization for Standardization (ISO) and the International Electrotechnical Commission (IEC).

Copies of *A Review of U.S. Participation in International Standards Activities* (NBSIR 88-3698) are available for \$14.95 prepaid from the National Technical Information Service, Springfield, VA 22161. Order by PB#88-164165.

FIRST MEASUREMENTS OF ULTRA-COLD ATOMIC COLLISIONS

NBS researchers working in collaboration with The University of Maryland (UM) have used a new “laser trap” to hold and cool large numbers of atoms, and make the *first measurements of an atomic collision process at ultra-cold temperatures*—within one thousandth of a degree of absolute zero. Collision processes underlie our understanding of large parts of physical chemistry. Ultra-cold collisions—which were impossible to study before the development of laser cooling techniques in the past several years—differ in fundamental ways from higher-temperature collisions; and offer *new insights* into the theory of atomic processes. The quantum-mechanical wave-like nature of the atoms, which is unimportant at higher temperatures, becomes of paramount importance in ultra-cold collisions. The results of the NBS/UM experiments in “Observation of Associative Ionization of Ultra-Cold Laser-Trapped Sodium Atoms,” appear in the Feb. 29 *Physical Review Letters*.

NBS FINDS DAT COPY-PREVENTION SYSTEM DEFICIENT

An encoding system proposed by CBS Records to *prevent prerecorded music from being copied by new digital audio tape (DAT) recorders is inadequate on three counts*, NBS concluded after a 5-month study at the request of the U.S. Congress. Specifically, NBS found that “the system does not achieve its stated purpose” because it sometimes permits the recording of material that is encoded to prevent copying and sometimes inhibits the recording of material that is not encoded. Listening tests showed that for some listeners and some musical selections, inclusion of the copy-prevention code in recorded material makes a “discernable difference.” In addition, NBS found that the copy-prevention system can be bypassed easily.

The work was in part funded by two groups concerned with this issue, the Home Recording Rights Coalition and the Recording Industry Association of America.

Copies of the NBS report, *Evaluation of a Copy Prevention Method for Digital Audio Tape Systems* (NBSIR 88-3725), are available for \$25.95 (\$51.90 for foreign mailing) from the National Technical Information Service, Springfield, VA 22161, telephone: 703/487-4650. Request PB#88-169537.

NEW TELEPHONE SERVICE TO SET CLOCKS IN COMPUTERS

NBS is initiating an Automated Computer Time Service (ACTS) to allow *automated checking or setting of clocks through commercial telephone lines*. Computers, whether personal microcomputers or huge mainframes, often need to have their internal clocks accurately set to the time of day. For example, seismological and astronomical data need to be accurately tagged with time and date. The new service will provide accuracy levels between 1/10 and 1/1000 second (depending on mode). The service will be in a test phase for the first 6 months, with NBS soliciting comments on format and operation. The telephone number for modem dial-up initially is 303/494-4774.

Documentation of the service, instructions on how to use it, and example programs to set personal computer clocks (on a 5 1/4-inch, 360-kilo-byte DOS diskette) are available for \$35 prepaid from the Office of Standard Reference Materials, B311 Chemistry Building, National Bureau of Standards, Gaithersburg, MD 20899, telephone: 301/975-6776. Specify “Automated Computer Time Service (ACTS), RM 8101.”

IMPROVING AIRCRAFT SAFETY IS GOAL OF JOINT FEDERAL RESEARCH PROJECT

Safer aircraft takeoffs and landings are the aims of a joint project by the National Bureau of Standards (NBS) for the Federal Aviation Administration (FAA).

Navigation and landing aids often are placed on structures on or near airport runways. To reduce damage from possible collisions with these structures, the FAA and the Transportation Systems Center, a Department of Transportation administration office, have investigated “breakaway” structures. These “Low Impact Resistance Structures” (LIRS) are intended to sustain environmental loads, such as high winds, yet break apart easily if struck by a lightweight aircraft.

Researchers in the NBS Center for Building Technology are developing computer models to simulate what happens when an aircraft collides with such a structure. At present, the only way to test a design is by building a full-scale model, simulating a collision, and observing how well the design works. These tests are expensive, only give information on a particular design, and do not take into account environmental conditions.

The NBS researchers are using the bureau's large-scale structural test facility to simulate the forces of jet blast and the environmental loads these structures are exposed to. The computer models being developed by NBS for this project will be evaluated and validated using data from these tests. The first structure being tested is a prototype breakaway tower 20-feet high by 10-feet square. The tower was designed by the project members and fabricated by Jaquith Industries of Syracuse, using a fiberglass-reinforced plastic material. After the environmental load tests are completed at NBS, the structure will be shipped to a crash test facility selected by FAA.

In other testing, Richard Fields of the NBS Metallurgy Division has evaluated the behavior of electrical cables located inside the breakaway structures. During a collision with an aircraft, these cables can cause considerable damage unless they also "break away." Under a simulated aircraft impact, Fields measured the energy and forces required to break through the cables. He then tested the strength of the cables spliced with commercially-available connectors designed to give way when struck. Fields found that the cables with the connectors were strong enough to sustain environmental loads and yet easily fell apart during a simulated collision.

Standard Reference Materials

NEW SAMPLES TO AID IN MEASURING CHOLESTEROL, VITAMINS

A standard reference material (SRM) to help laboratories measure several *nutrients—fat-soluble vitamins as well as cholesterol—in food products* is now available from NBS. The packaged material combines known quantities of the nutrients in coconut oil, a natural fat product used in the preparation of many foods such as infant formula. Food chemists and nutritional scientists should find the material useful as a standard to check the operation of laboratory equipment as well as to develop and validate methods for analyzing some fat-based food samples. Each SRM contains 10 vials of material: five have natural coconut oil only and five are fortified with certified levels of cholesterol, vitamin E (as dl-alpha-tocopheryl acetate), vitamin A (as retinyl acetate), and vitamin D₂ (ergocalciferol).

The material, SRM 1563, is \$181 from the Office of Standard Reference Materials, B311 Chemistry Building, National Bureau of Standards, Gaithersburg, MD 20899, telephone: 301/975-6776.

Standard Reference Data

NEW DIFFRACTION AND CRYSTAL DATABASES AVAILABLE

Analytical chemists in industry, universities, and government will be interested in two new computerized standard reference databases for use in identifying the structures in materials. The *NBS/Sandia/ICDD Electron Diffraction Database*, developed by the bureau, Sandia National Laboratory, and the International Centre for Diffraction Data (ICDD), contains evaluated data for more than 70,000 inorganic substances. It is an important *analytical tool for researchers using electron microscopes to identify unknown substances*. The *NBS Crystal Database* contains complete crystallographic and chemical data on more than 120,000 compounds. In addition to its use in identifying unknown crystalline materials, the software program permits chemical data to be combined with crystal structure information to solve many chemistry problems.

Both databases are available for lease in a variety of formats, including tapes and disks, from the International Centre for Diffraction Data, 1601 Park Lane, Swarthmore, PA 19081, telephone: 215/328-9400.

For information on the NBS Standard Reference Data Program, write or call: Office of Standard Reference Data, A323 Physics Building, National Bureau of Standards, Gaithersburg, MD 20899, telephone: 301/975-2208.

Calendar

October 17–20, 1988

**11th NATIONAL COMPUTER SECURITY
CONFERENCE
COMPUTER SECURITY... INTO
THE FUTURE**

Location: Baltimore Convention Center
Baltimore, MD

This conference provides a forum for the Government and the private sector to share computer security information, offering multiple tracks that address technical, management, and special topics. A Call for Papers has been issued requesting papers be submitted on the following topics: Building Secure Applications, Innovations and New Products, Research and Development, Evaluation and Certification, Integrity and Availability, Management and Administration, and Security Education and Training. By *February 15, 1988*, prospective authors should send five copies of a draft paper, including author's name, address, and telephone number, to Computer Security Conference, c/o Robyn Winder, ATTN: C1, National Computer Security Center, 9800 Savage Road, Fort George G. Meade, MD 20755-6000. Speakers selected to participate in the conference will be notified by April 30, 1988; final, camera-ready papers are due by June 30.

Sponsored by the National Bureau of Standards and the National Computer Security Center.

For further information on paper submissions, contact Robyn Winder, at the address above, or at 301/859-4450. For further technical information, contact Eliot Sohmer, ATTN: C1 National Computer Security Center, 9800 Savage Road, Fort George G. Meade, MD 20755-6000, 301/859-4450 or Irene Isaac, B266 Technology Building, National Bureau of Standards, Gaithersburg, MD 20899, 301/975-3360.

October 19–21, 1988

**CLINICAL LABORATORY
MEASUREMENTS:
ACCURACY AND PATIENT NEEDS**

Location: National Bureau of Standards
Gaithersburg, MD

Improving clinical accuracy of four kinds of tests—for the AIDS virus, cholesterol, drugs of abuse, and cervical cancer (Pap smears)—is the aim of this seminar. Thirteen industry, federal, and professional organizations, which together represent nearly every facet of the clinical laboratory and medical communities, have joined forces to sponsor the seminar as an opportunity to address key measurement issues and as a response to sustained concern among Congress, the news media, and the general public about laboratory testing issues. The seminar will include general discussions of both theoretical and practical approaches to measurement systems. A legislative viewpoint of clinical measurements also will be included. “Challenge speakers” will present a slate of accuracy issues, each of which will be analyzed by one of four working groups in breakout sessions. Recommendations will then be offered for comment to seminar participants and finally will be proposed to the National Committee for Clinical Laboratory Standards for consensus evaluation.

Seminar sponsors are: American Association for Clinical Chemistry; American Clinical Laboratory Association; American Medical Association; American Medical Technologists; American Society for Medical Technology; American Society for Microbiology; American Society of Clinical Pathologists; Centers for Disease Control; College of American Pathologists; Health Industry Manufacturers Association; National Bureau of Standards; National Committee for Clinical Laboratory Standards; and the National Institutes of Health.

Contact: Dr. Harry S. Hertz, A309 Chemistry Building, National Bureau of Standards, Gaithersburg, MD 20899, 301/975-3145.

April 17–23, 1989

**NUCLEAR ANALYTICAL TECHNIQUES
IN THE LIFE SCIENCES**

Location: National Bureau of Standards
Gaithersburg, MD

Nuclear analytical techniques, in particular activation techniques (commonly referred to as activation analysis), constitute an important group of methods of chemical and physical-chemical analysis. This is the fourth symposium in a series on the subject of nuclear activation analysis. Activation analysis has been particularly important in providing data on the trace and ultratrace elements and increasingly sophisticated analytical methods are employed to search for new answers. This meeting will review some of the more recent developments in the field and provide a viewpoint on the current status of nuclear techniques. The meeting organizers are inviting scientific contributions that are related to the analytical utilization of nuclear techniques. Papers will be presented in oral sessions on the following topics: (1) New and Emerging Methodology, (2) Activation Techniques, (3) Quality Assurance, (4) Comparison of Activation Analysis with Other Methods and (5) Applications of Nuclear Techniques in biology, medicine, biotechnology, agriculture, and nutrition as well as in public and environmental health.

This international conference is sponsored by the National Bureau of Standards, the American Nuclear Society, and the International Atomic Energy Agency.

Contact: Rolf Zeisler, B108 Building 235,
National Bureau of Standards, Gaithersburg,
MD 20899, 301/975-6290.

An Improvement in the Reliability of Standard Cell Enclosures

Volume 93

Number 4

July–August 1988

Bruce F. Field and Liu Ruimin¹
National Bureau of Standards
Gaithersburg, MD 20899

We describe the design of a new temperature-regulation circuit, which is used as an outer oven controller for new standard cell enclosures, with the emphasis on improving the reliability of the temperature control. A redundant protection circuit is used to prevent loss of temperature control caused by component failures in the controller. The temperature control of the outer oven of the enclosure is better than 0.4 mK per °C change in ambient temperature. When used with the additional inner controller the sensitivity of the cell

temperature to the ambient temperature is improved to 20 $\mu\text{K}/^\circ\text{C}$. This paper describes in detail the new circuit, summarizes the enclosure construction, and presents data on the performance of the system.

Key words: reliable temperature controller; standard cell enclosure; temperature protection circuit; temperature-regulated oven.

Accepted: February 18, 1988

1. Introduction

If saturated standard cells are to be used as a high precision voltage reference, they must be kept in a constant temperature-regulated oil bath or air enclosure because of their large temperature coefficient of EMF. The requirements for such an enclosure are good temperature stability and high reliability of the temperature control circuit. The importance of the reliability requirement is often overlooked. If the enclosure (and cell) temperature changes significantly (several degrees Celsius), the chemical equilibrium within the cell is disturbed and after control is re-established it may still take several weeks or months for the cell EMFs to recover to their original values. Sometimes an unpredictable permanent change in the cell EMFs can also occur. Recently, two new standard cell enclo-

tures have been constructed with the emphasis on reliability of the temperature control circuitry. The new enclosures are similar to two older standard cell enclosures, previously constructed at NBS in 1974, but the controller circuitry has been redesigned to be more reliable and to replace obsolete components [1]. One problem has been that the extensive protection circuits used in the original enclosures contain several components that fail routinely. The concern for improved reliability has led to the development of redundant protection circuits in the new enclosures to prevent loss of temperature control caused by component failures in the controller.

The mechanical construction details of the new enclosures are the same as for the previous enclosures, i.e., they consist of four concentric aluminum cylinders separated by formed polystyrene insulation with two of the four cylinders controlled by

¹Liu Ruimin was an NBS guest scientist from the National Institute of Metrology, Beijing, China.

an outer oven controller and an inner oven controller. As in the original design, the outer cylinder is unheated and thermally lags the enclosure from ambient temperature changes. The next two cylinders are the outer heater and inner heater, respectively, with the last cylinder being a temperature lagged cell compartment to further reduce any temperature gradients. However, the original controller circuitry has been changed completely. A simple control circuit using a platinum resistance thermometer with chopped-dc excitation and phase sensitive detection developed by Cutkosky and Davis is used as the inner oven controller [2]. The outer oven controller contains a main controller, a backup controller, and an arbitration circuit that connects the outer oven heater to the main controller or to the backup controller in the event of main controller failure. This paper describes the outer oven controller and protection circuitry and presents data on the performance of the system.

2. Circuit Details

The enclosure is designed for an inner oven temperature of 30 °C with the outer oven set to

29.9 °C. Thus, the outer oven provides most of the power, 4 W with an ambient temperature of 23 °C, while the inner oven typically supplies 75 mW with a maximum output capacity of 300 mW. Because of the limited power capacity of the inner oven (and the correspondingly limited temperature increase), guaranteeing the integrity of the outer oven is sufficient to prevent extreme changes in the inner oven temperature even in the event of an inner oven failure.

2.1 Outer Oven Controller

The main controller and backup controller for the outer oven are nearly identical control circuits using independent thermistor sensors in Wheatstone bridges and high-gain dc amplifiers to provide proportional temperature control (see fig. 1). Power to each controller is supplied by its own independent well-regulated power supply. The outer oven temperature (for each controller) is monitored by a thermistor (10 kΩ @ 25 °C) mounted in a small hole drilled in the enclosure and filled with silicon heat sink grease. The thermistor forms one arm of a nearly equal-arm Wheatstone bridge powered by a low-voltage derived from the regulated power supplies. The output of the bridge

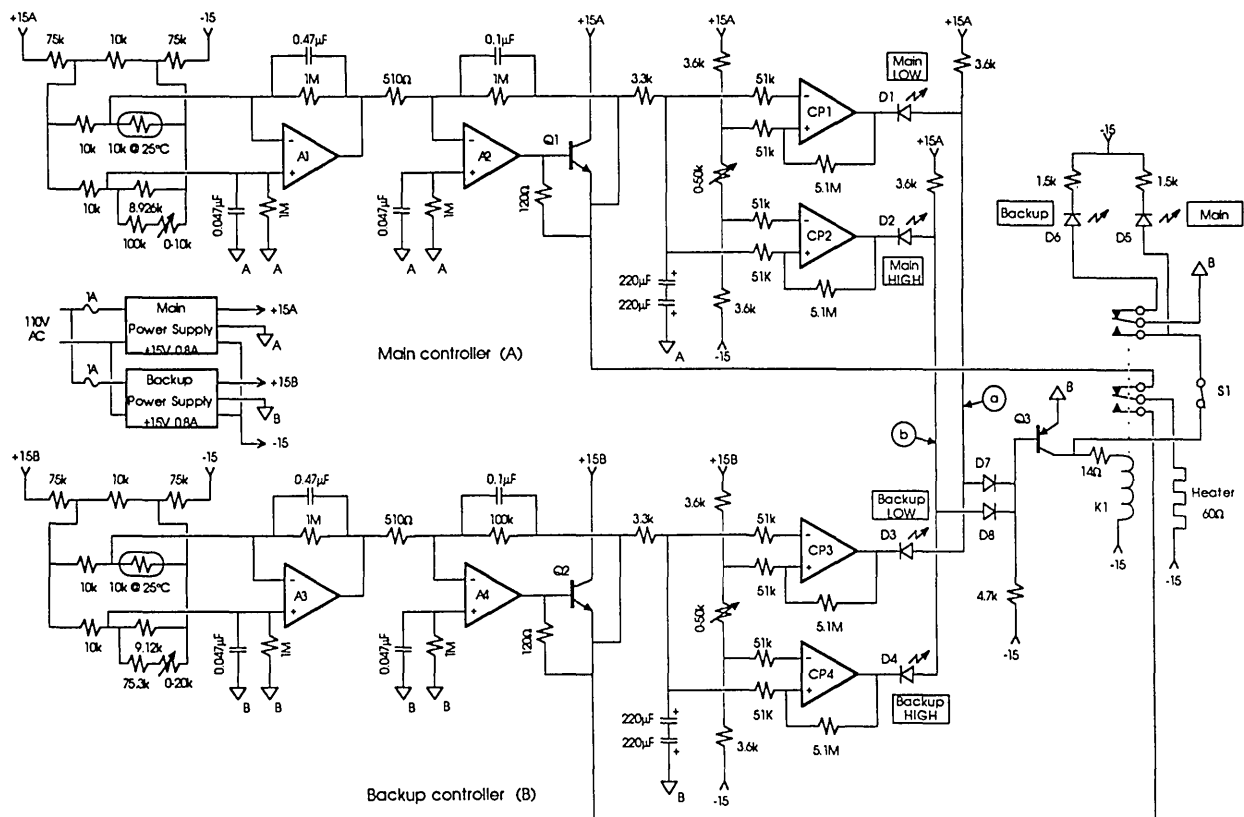


Figure 1. Circuit diagram of the outer oven controller.

is amplified by a two-stage low-offset-voltage dc amplifier which in turn drives a transistor to boost the output for the 60- Ω heater.

The arbitration circuit consists of four voltage comparators, a transistor and a sensitivity relay. This circuit determines which controller is operating correctly and switches the proper controller output to the outer oven heater. Each controller output is compared to a high and low limit using two comparators. The high and low limits are set to ± 10 V for the main controller and ± 5 V for the backup controller. The outputs of the controllers exceed either of the limits only if a controller has failed or the enclosure is warming up from ambient temperature. Under normal conditions when the controller outputs are within the limits, the output voltages of the four comparators CP1-CP4 are high (see fig. 1). The four diodes, D1-D4, are cut off and the potentials of points a and b are high, turning on diodes D7 and D8 and forcing the transistor Q3 to be turned off and the relay to be released. The main controller output is thus connected to the outer oven heater. This arrangement extends the life of the relay and transistor Q3 because they are normally not operated.

If the main controller were to fail due to a faulty component and supply no power to the heater while the backup controller continued operating properly, the output of comparator CP2 would go low and diode D2 would turn on. As the temperature of the enclosure drifted down eventually CP3 would go low turning on diode D3, forcing potentials a and b low, and causing the relay to operate. A similar sequence occurs if the main controller

were to fail and supply full power to the heater. The logic requires that both controllers indicate that the enclosure temperature is out of control and to disagree as to the direction (high or low) before switching to the backup controller. This permits the enclosure to warm from room temperature without switching to the backup controller. Once the backup controller has gained control the second set of contacts on the relay provide a self-locking arrangement to keep the relay energized. The control can be returned to the main controller only by opening switch S1 manually. A failure of the backup controller has no effect on the operation of the circuit as long as the main controller operates normally. Table 1 summarizes all the failure conditions and the status of the relay.

Diodes D1-D6 are light emitting diodes mounted on the front panel of the controller to indicate the status of the outer oven temperature control. One of the advantages of this design is that a failure of the backup controller can be discovered immediately by observing the light emitting diodes, even if it is not the active controller.

The main and backup controllers differ only with respect to the total circuit gain, with gains of 2.17×10^5 and 2.17×10^4 , respectively. The gain of the main controller was empirically determined for good regulation and rapid recovery from ambient temperature changes. The gain of the backup controller was deliberately set lower to avoid a conflict between the controllers due to their temperature set points drifting apart. It should be noted that for proper operation the control temperatures (set points) of the main controller and

Table 1. Operating Conditions and Status of the Outer Oven Controller

Output of		Output of Comparators				Potential of		Relay Condition	Status of Controller
A	B	1	2	3	4	a	b		
Normal	Normal	1	1	1	1	1	1	released	A, B operating normally
Normal	Low	1	1	1	0	0	1	released	B failure
Normal	High	1	1	0	1	1	0	released	B failure
Low	Normal	1	0	1	1	0	1	released	Probably warming from ambient temp. if A fails, B will eventually go high
High	Normal	0	1	1	1	1	0	released	Probable A failure, B will eventually go low
Low	Low	1	0	1	0	0	1	released	Warming from ambient temp.
High	High	0	1	0	1	1	0	released	Ambient temp. exceeds control temp.
Low	High	1	0	0	1	0	0	operated	A fails, control transferred to B
High	Low	0	1	1	0	0	0	operated	A fails, control transferred to B

A ---- Main controller. B ---- Backup controller. 1 ---- High level voltage. 0 ---- Low level voltage.

backup controller must be carefully adjusted to the same value. This was accomplished when the enclosures were first put under test by adjusting the trim resistor on the backup controller, which parallels an arm of the bridge, to equalize the outputs of the controllers. Under normal operating conditions a change in the set point of the main controller of $5 \text{ m}^\circ\text{C}$ (due to a drifting resistor in the bridge for example) would cause a negligible change in the amplifier output to the heater, while the voltage output of the backup controller would change 1 V . With the currently set limits of the comparators the two controller set points can drift apart as much as 0.025°C (and this is considered to be an unlikely occurrence) before a failure is indicated.

2.2 Inner Oven Controller

The inner oven is held at a temperature of 30°C , approximately 0.1°C higher than the surrounding outer oven. The heater voltage is indicated on a meter mounted on the front of the controller and the outer oven temperature is adjusted so the inner oven output voltage is at mid-scale ($\approx 75 \text{ mW}$ which corresponds to a 0.1°C temperature rise). A platinum resistance thermometer ($110 \Omega @ 30^\circ\text{C}$) was chosen as the sensor because of its excellent long-term stability, although its temperature coefficient is much smaller than that of the thermistor and the output of the bridge is only 63.3 nV/mK . In order to avoid the effects of dc voltage offsets and drifts in a dc amplifier circuit, a circuit consisting of a chopped dc amplifier and a phase sensitive detector was chosen [2]. Its output is used to drive a 3000Ω -heater via a current booster. An additional power supply, separate from the ones used for the outer ovens, is used to power the circuitry. It has been proven experimentally that the circuit will meet our requirement for high-stability temperature control with day-to-day variations of less than $50 \mu\text{K}$. Since the enclosure is a system with large thermal inertia, the time constant of the controller feedback must match it. Figure 2 shows the temperature of the inner controller in one of the enclosures in response to a perturbation with different values of capacitance in the feedback loop. From these curves we calculated an optimum value for the capacitance for fast recovery and long term stability.

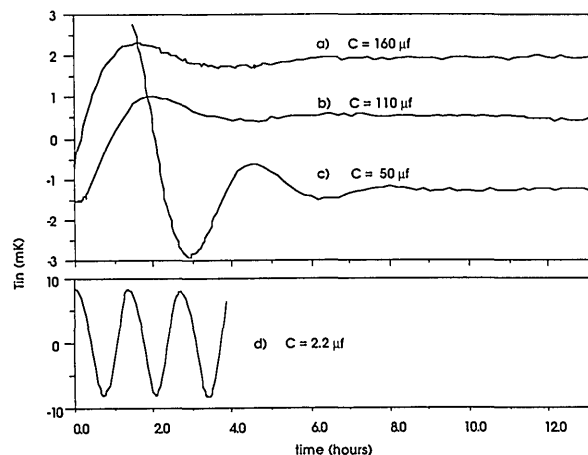


Figure 2. Response of the inner oven controller to a temperature perturbation for various values of feedback capacitance. Curves a–c are from one enclosure, d is from the second enclosure.

3. Performance

In order to test the stability of temperature control of the enclosures with a changing ambient temperature, the enclosures were placed in a temperature-controlled chamber and the temperature was changed in the sequence 24°C , 28°C , 24°C , 20°C , 24°C . The enclosures were held at each temperature for one or two days. The outer oven temperature was monitored by measuring the output of the backup controller. A plot of the outer oven temperature change with ambient temperature for one of the enclosures is shown in figure 3. The change of the outer oven temperature with the ambient temperature is not linear because it is pro-

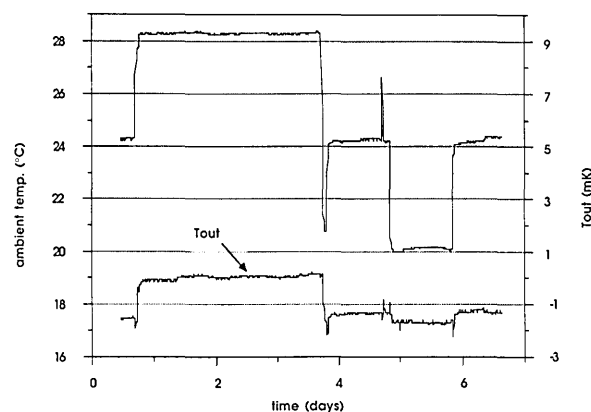


Figure 3. Outer oven temperature change with the ambient temperature for one of the enclosures.

portional to the square of the output voltage of the outer oven controller. The result is that the variation of the outer oven temperature is less than 400 μK for ambient temperature changes of 1 $^{\circ}\text{C}$. The maximum temperature excursion over a period of more than fifty days was found to be less than 1 mK.

The temperature of the cell compartment of the enclosure is monitored by two thermistors mounted in a hole in the bottom of the compartment. The thermistors (10 k Ω @ 25 $^{\circ}\text{C}$) are connected in opposite arms of a Wheatstone bridge with two low-temperature-coefficient resistors (10 k Ω) in the other arms. The low-temperature-coefficient resistors are contained within the outer oven to further improve their stability. The bridge is powered from the regulated power supply of the inner oven. The output of the bridge is 4.155 mV/ $^{\circ}\text{C}$ with only 1.37 μW dissipated in each thermistor. The output is measured directly by a nanovoltmeter or a high-resolution DVM. For the following measurements a DVM was used that had a short term measurement noise of 0.02 μV , which corresponds to 5 μK . As shown in figure 4 the variations of the cell compartment temperature as measured by this thermistor bridge are less than 20 μK for ambient temperature changes of 1 $^{\circ}\text{C}$.

aberration to the cell temperature and a failure can be detected immediately so that corrective action can be taken. In addition, the circuitry has been simplified over the original design, thus greatly reducing the possibility of a failure. Despite the simplicity of the outer oven controller it can be used alone to obtain temperature control with a stability of 1 mK or, as shown here, it can be used with an additional inner controller to provide even better stability.

About the authors: Bruce F. Field is an electrical engineer in the Electricity Division of the NBS Center for Basic Standards. Liu Ruimin is with the National Institute of Metrology, Beijing, China and was a guest worker at NBS.

References

- [1] Cutkosky, R. D., and Field, B. F., IEEE Trans. Instrum. Meas. 23, 295 (1974).
- [2] Cutkosky, R. D., and Davis, R. S., Rev. Sci. Instrum. 52, 1403 (1981).

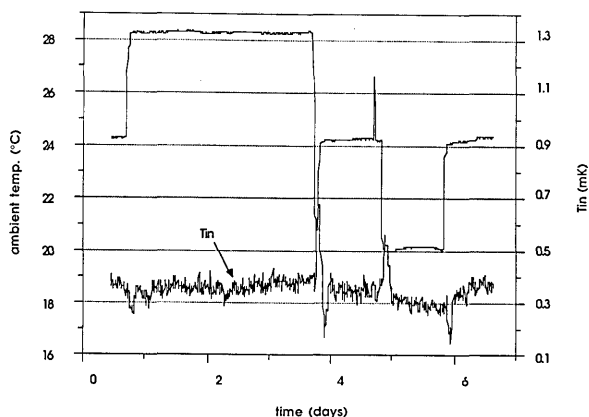


Figure 4. Variation of the cell compartment temperature with the ambient temperature in one of the enclosures.

4. Conclusions

We have demonstrated that with a small amount of additional circuitry a substantial improvement can be made in the reliability of a temperature controller. With this design, a failure of any one component will not cause a significant

The NBS Vision System in the AMRF

Volume 93

Number 4

July–August 1988

**Marilyn Nashman
and Karen J. Chaconas**

National Bureau of Standards
Gaithersburg, MD 20899

This article describes the NBS Vision System developed by the Sensory Intelligence Group of the Robotics System Division which is used in the Automated Manufacturing Research Facility (AMRF). It discusses the objectives of the Vision System and its applications in the factory environment. Since the Vision System is a multi-processor system, each process is described according to its position in the vision hierarchy as well as to its particular logical and computational functions. The interfaces between the individual processes of the Vision System and the interfaces between the Vision System and other

AMRF systems are described. AMRF documentation packages describing the Horizontal Workstation, the Real-Time Control System and the Material Handling Workstation are available from the Center for Manufacturing Engineering.

Key words: Automated Manufacturing Research Facility; computer vision; hierarchical design; image processing; Material Handling Workstation; multi-processor; real-time; Real-Time Control System.

Accepted: March 10, 1988

Introduction

The use of real-time sensory feedback in the manufacturing work place adds the dimension of intelligence to automated tasks. With the use of specially mounted cameras, visual information extracted from a scene is made available to the appropriate Automated Manufacturing Research Facility systems. This information enables robot control systems and planners to react appropriately to the tasks and objects in their environment.

The NBS Vision System is an industrial parts recognition system which operates in real-time. It is a model based system which recognizes parts by matching an input image with a set of predefined models of parts. Models of a known set of industrial parts, computed in advance, reside in a database and are used to identify each instance of an object and to specify its position and orientation

relative to a fixed camera configuration. This system is particularly suited for a factory application because the number of parts to be identified is small, the parts can be exactly specified with known tolerances on the dimensions, and the features of the parts, e.g., corners, holes, etc., are distinctive.

The NBS Vision System serves two sub-systems of the AMRF: it is used both in the Horizontal Workstation (HWS) and the Material Handling Workstation (MHWS). In the HWS, vision is used to confirm or reject the identity of a machine part and to compute the position and orientation of confirmed parts. In the MHWS, vision is used to verify the contents of trays being delivered between workstations.

Physical Description of the NBS Vision System

The NBS Vision System accepts images from a camera mounted on the wrist of a manipulator at the HWS as well as a stationary camera mounted on an inspection gantry in conjunction with the MHWS. Figure 1 describes the AMRF floor plan and the physical location of the NBS Vision Sys-

tem in the factory. Both cameras are electronically attached to a hardware circuit that converts the incoming signals into black and white images and compresses that information as it is read. All visual information is extracted by analyzing this resultant binary image.

The manipulator camera used at the HWS is fixed on the robot wrist. Below the camera, at a known distance from it, a light source is also at-

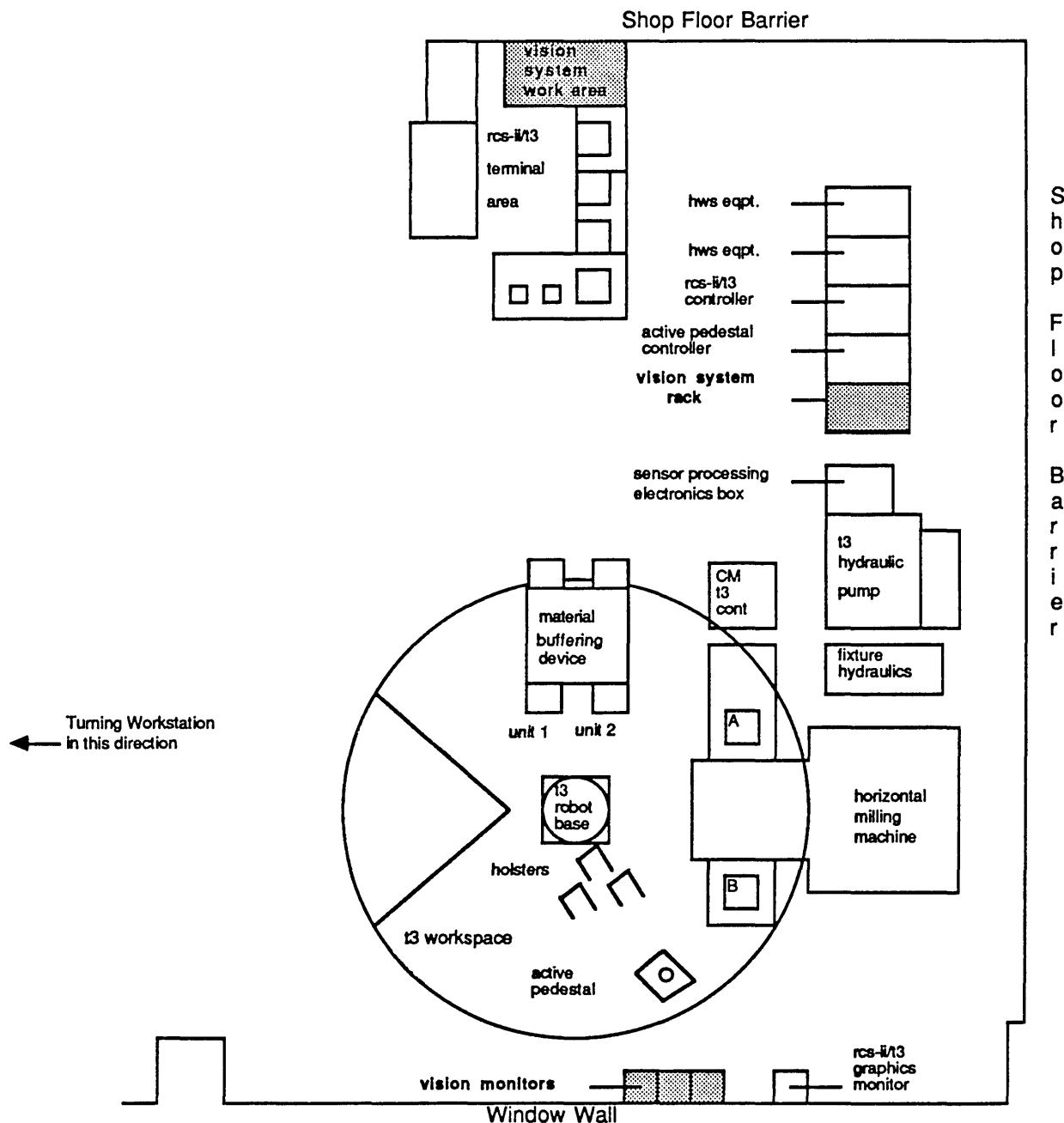


Figure 1. AMRF shop floor.

municates with other processes via a pre-defined common memory block. System routines have been developed to insure the integrity of this data transfer (fig. 4).

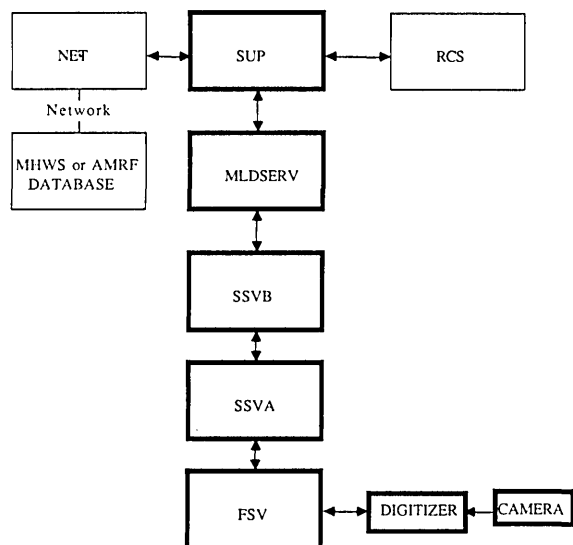


Figure 4. NBS vision system.

Three of the processes operate in a bottom-up mode to read an image and globally extract information from it. These processes are First Stage Vision (FSV), Second Stage Vision A (SSVA), and Second Stage Vision B (SSVB). A fourth process, the Multi-Level Database and Server (MLDSERV), acts in a top-down mode using its database of models to identify specific objects in a scene. The Supervisor Process (SUP) monitors Vision System activity and receives commands from other AMRF systems via the Netboard (NET) processor. Commands for vision processing are passed from SUP to the Server which determines what a command is requesting and how to answer it.

There are currently four types of requests to which the Vision System responds. In all cases, information is supplied only when commands from either the RCS or the MHWS are received. The three questions posed by the RCS include a request for the position of the centroid of the object in view; a verification of a specific factory part in a scene, and if verified, the position and orientation of that part; and lastly, the computed range to the surface of the object in view. The answers supplied by the Vision System enable the RCS to compute the required robot motion to position the manipulator and plan a trajectory for picking up the verified object at the optimum grasp point.

The fourth type of question to which the Vision System responds is posed by the MHWS and is a request for verification of the contents of a tray of parts being delivered between AMRF workstations. Through the AMRF database, the MHWS supplies information regarding the intended contents of a particular tray, e.g., the number of parts contained in the tray and the sectors of the tray in which particular parts are expected to be located. By analyzing the image of the tray and comparing the actual tray's contents with the internal model database, this information is either confirmed or rejected. A tray which fails verification is not processed further.

Hierarchy of the Vision System

First State Vision is the lowest level in the vision processing hierarchy and acts as the interface between the camera hardware and the Vision System. It receives requests for raw image information from Second Stage Vision A and translates those requests into camera hardware commands. It then reads a compressed form of the camera image and transfers it to the appropriate common memory locations.

FSV controls the commands sent to the frame-buffer, which converts analog signals from the camera into digital intensity information. The resultant image is a rectangular array of image data or pixels which are assigned integer grey levels depending on their measured brightness. Thresholding converts these grey levels to two colors, black or white, depending on whether an individual pixel value is less than or greater than the given threshold value. The binary image is converted to run-length encoded information, a compressed data representation which records only transitions from black to white or white to black (fig. 5), and is read and stored by FSV.

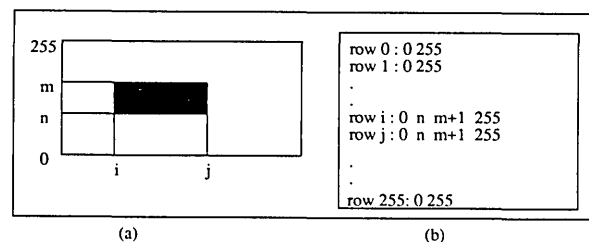


Figure 5. Data representation. (a) Binary image. (b) Run-length representation.

tached to the wrist. The light source is able to generate two kinds of light flashes. The first is a flood flash that illuminates the whole field of view of the camera while the second light source generates two parallel planes of light which illuminate those points in the field of view that intersect the planes of light (fig. 2) [1].

The flood flash is used to find shape features such as the outlines of objects in two dimensions. The structured light is used to compute the pitch and yaw orientations of simple geometric surfaces and the range to objects. A combination of structured light and flood flash enables the system to extract elevation, azimuth, and roll orientation of the illuminated surfaces (fig. 3) [2].

The camera mounted on the inspection gantry is provided with flood lights rather than a flash.

Since this is a fixed configuration, the range to the objects in the scene is always known and thus only two dimensional shape features are required for analysis.

Overview of the NBS Vision System

The NBS Vision System is designed in a hierarchical manner: commands from both the MHWS and the Realtime Control System (RCS) operating in the HWS are decomposed into lower-level tasks and executed by appropriate levels of the system. There are currently six independent processes operating asynchronously which analyze and extract information from an image scene. Each process resides on its own microprocessor board and com-

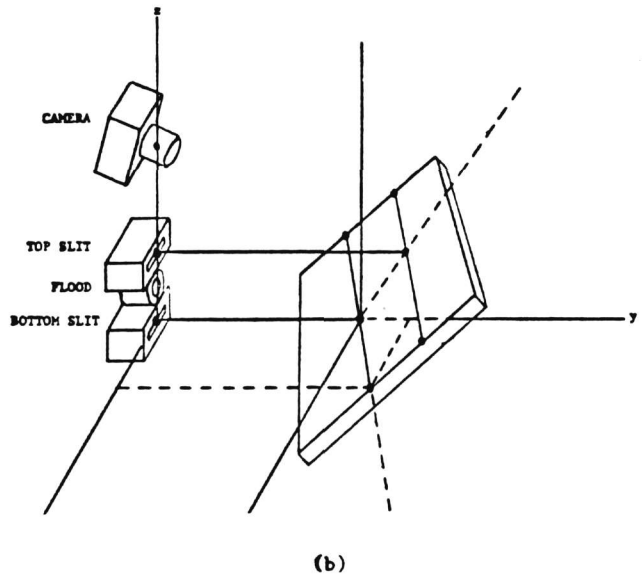
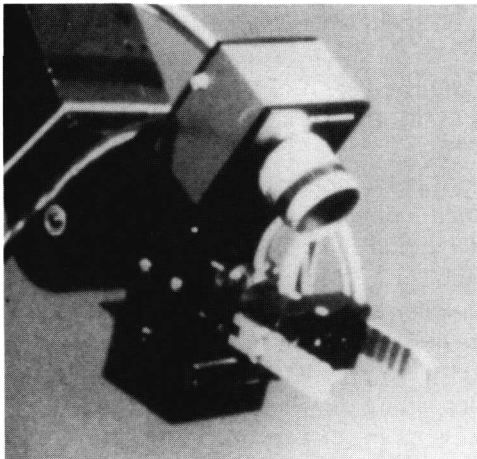


Figure 2. (a) Camera and light source mounted on the manipulator. (b) Relationship between the camera and the light sources.

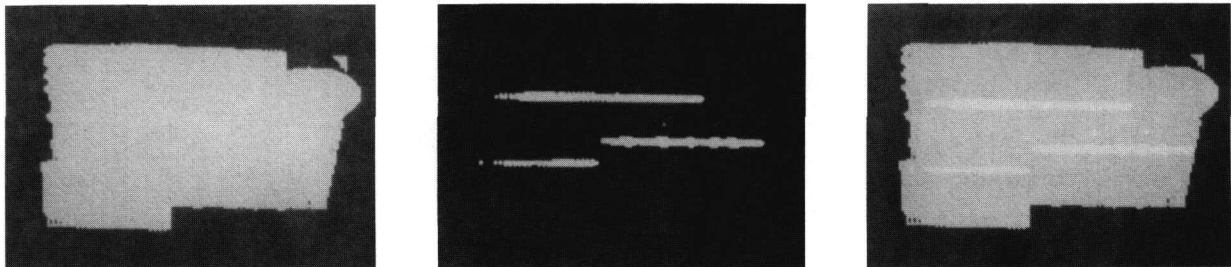


Figure 3. Left: Binary image of an object as seen under flood lighting. Center: Object as seen using the plane of light. Right: The two images superimposed.

SSVA receives its commands from the next higher level of the hierarchy, SSVB. It waits for FSV to read in an image and then reads the run-length encoded data from a predefined common memory area. SSVA performs different operations on the incoming data depending on the kind of picture (flood or structured light) that has been requested.

On receiving picture data from a floodlit image, SSVA performs a connected components analysis [7] and constructs a list of the objects (blobs) in the image. It also computes various properties of each blob such as the area, centroid, moments, etc. and encodes all points on the boundary. When the image results from using parallel planes of light, SSVA constructs groups of connected curve segments [7]. The segments correspond to single curves or to pieces of curves starting where a curve splits and ending when it ends or merges with another curve. The results of these computations are passed to SSVB by storing the structures into another common memory block.

SSVB receives commands from the first level of the Multilevel Database Processor (MLDSERV) and passes them down to SSVA. Upon receiving the data structure of blobs or curves in the image, it performs feature analysis on each object in the image. For floodlit images, this involves finding the corners, principal axis, number of holes, and perimeter of each object. For structured light images, each segment is described in terms of a polynomial and the endpoints. SSVB sends the list of objects and a set of structures describing the features to MLDSERV and then waits until another command is received.

In addition to acting as the Vision System database, MLDSERV is also the module which performs recognition and matching tasks. As a database, it stores the results of the lower-level processing in structures appropriate for the upper-level recognition algorithms. It also contains a database of statistical information which has been computed a priori describing attributes of all parts to be accessed by the RCS and the MHWS. The Server is the portion of MLDSERV which interprets commands received by SUP and formulates an answer to the questions posed. Its main activities are concerned with recognizing objects and extracting relevant information from the database. In addition, this module performs some of the range and position computations and is responsible for driving the graphic output displays.

SUP is considered to be the “brains” of the Vision System. It accepts commands from either the

RCS or the MHWS, interprets them, translates them into a form suitable for the Vision System, and initiates the command sequence in the Vision System. If a poor quality image is detected, SUP tries to adjust the camera parameters to improve the picture and then repeats the process. If there are no processing errors, it sends the appropriate status and answers to either the RCS or the MHWS. In addition, SUP checks that each of the vision levels is working and monitors the terminal keyboard to service interactive features useful for providing information to the human operator.

System Interfaces

The Vision System processes interface with each other using a common memory area governed by a file system. The interprocess communications are handled using a library of system routines developed at NBS [6]. The purpose of the library is to ensure data integrity of communications and to allow for asynchronous communications between processes. Blocks of common memory, called “files”, which are accessible to each vision process are defined. Flags associated with each file record the current state of each file. The state of a file includes information about the process which owns the file, the status of the file (open or closed), the last process which accessed the file, and the system time of last access. Only those processes granted read and/or write permission can access a file, and a process can only access a file if it is closed. The concept of opening and closing files is analogous to UNIX file system calls [4].

Communications between the RCS and the Vision System are handled using a microprocessor communications board. A master-slave relationship is represented on the board to describe the relationship between the two systems and to indicate the direction of communication. Communication is initialized by the RCS and protocols and command structures are used to allow the RCS to request service and to receive the necessary information from the Vision System.

The MHWS and the Vision System communicate using the VAX common memory mailbox system [5]. Mailbox areas are established when network communications are made to provide for message passing between systems. The Vision System queries the mailbox command area for a change in sequence number to detect when a tray verification request has been sent. Upon comple-

tion of the recognition task, a status report is sent to the MHWS mailbox to close the transaction.

Conclusion

The NBS Vision System is currently being used in the AMRF to provide sensory information to the Realtime Control System and the Material Handling Workstation. Inputs are interpreted by a hierarchically organized group of microprocessors. The system uses knowledge of object prototypes to provide real-time feedback to the robot control system and to verify the contents of trays of machine parts. Planes of light and flood light sources are used to quickly obtain the six degrees of freedom of an object relative to the robot. The Vision System is then able to interpret an object's 2-D outline in 3-space and to locate its centroid and principal axis. This information is used to guide the robot's actions and trajectory as well as to identify specific parts.

About the authors: Marilyn Nashman and Karen J. Chaconas are computer scientists working in the Robot Systems Division of the Center for Manufacturing Engineering at the National Bureau of Standards. They are primarily involved in research and development of real-time image processing techniques.

References

- [1] Albus, J. S., Haar, R., and Nashman, M., "Real-Time Three Dimensional Vision for Parts Acquisition", Soc. Photo-Optical Instrum. Eng. **283**, 56 (1981).
- [2] Albus, J. S., Kent, E., Nashman, M., Mansbach, P., Palombo, L., and Shneier, M., "Six Dimensional Vision System", Soc. Photo-Optical Instrum. Eng. **336**, 142 (1982).
- [3] Chaconas, K., and Nashman, M., "The NBS Vision System in the AMRF", NBSIR 87-3684, 1987.
- [4] Kernighan, B. W., and Ritchie, D. M., The C Programming Language, Prentice Hall Inc., 1978.
- [5] Nanzetta, P., and Rippey, W., "Integration of the AMRF", to be published.
- [6] Mansbach, P., "Overview of the 'GRAMPS' Operating System", 1988, to be published.
- [7] Rosenfeld, A. R., and Kak, A., Digital Picture Processing, Academic Press, 1976.

International Comparisons of Pressure Standards: A Status Report

Volume 93

Number 4

July–August 1988

Charles R. Tilford
National Bureau of Standards
Gaithersburg, MD 20899

In 1979 four working groups were established to organize comparisons between the pressure standards of the different national standards laboratories. These comparisons cover the range 10^{-6} to 10^8 Pa. This report describes the progress of the different comparisons and summarizes the results where available.

Key words: international comparison; pressure standards; primary standards; round robins; vacuum standards.

Accepted: February 4, 1988

Introduction

In March 1979 representatives of 17 national standards laboratories met in Sevres, France under the auspices of the International Bureau of Weights and Measures (BIPM), to discuss pressure standards and metrology. A consensus was developed on several points: Pressure measurements are of major importance for both scientific endeavors and industrial enterprises; Although pressure is not one of the designated "base" units, it is in most cases maintained and promulgated in the same manner as the basic units; Comparisons of pressure standards between national laboratories have been very limited, and a systematic set of comparisons would be of great help in establishing confidence in the uncertainty analyses of the various national standards and in identifying problems; Progress is sometimes slowed because of the limited opportunities for pressure metrologists to meet and discuss problems and advances in the field, particularly in the medium pressure ranges.

As a result of these discussions four working groups were established, each with the primary task of organizing comparisons between the pres-

sure standards maintained at national standards laboratories. The four working groups were: High Pressures (1 to 100 MPa) with G. F. Molinar of the Istituto de Metrologia "G. Colonnetti", Turin, Italy, selected as Chairman; Medium or Barometric Pressures (1 to 1000 kPa) with P. R. Stuart of the National Physical Laboratory, Teddington, United Kingdom, as Chairman; Low Pressures (1 to 1000 Pa) with C. R. Tilford of the National Bureau of Standards, Gaithersburg, USA, as Chairman; and Very Low Pressures (10^{-4} to 1 Pa) with G. Messer of the Physikalisch-Technische Bundesanstalt, Berlin, German Federal Republic, as Chairman. The working groups separately met and began the tasks of identifying pilot laboratories, selecting transfer standards, and determining the number of intercomparison participants. Two years later, in June 1981, the International Conference on Weights and Measures (CIPM) established the Consultative Committee on Mass and Related Quantities (CCM), the related quantities being density, force, and pressure. The four pressure working groups established by the 1979 meeting were

incorporated as CCM working groups with their activities to continue as previously planned.

The status of the intercomparisons organized by the four working groups are summarized below. It is of interest that in all four cases the intercomparisons have been delayed and/or compromised by problems with the transfer standards. In all but the medium pressure case larger-than-expected instabilities have been discovered, and in the low pressure and very low pressure cases these instabilities exceeded the uncertainties of the standards to be compared.

High Pressures

The high pressure working group selected as an initial effort a comparison of pressure standards in the range 20 to 100 MPa. The Laboratoire National d'Essais (LNE), Paris, France, volunteered to act as the pilot laboratory. Two oil-operated simple piston gages were made available by a manufacturer for use as a transfer standard and backup. After characterization of the transfer gage and ancillary equipment, and selection of a pressure fluid (diethylhexylsebacate), the comparisons were initiated in phases using the "petal" scheme, i.e., measurements of the transfer standard were made by the pilot laboratory at the beginning and end of each phase, or set up calibrations by a group of participating laboratories.

To date, three phases, including 13 laboratories, have been completed. The participants, in addition to LNE, were: First phase, Istituto di Metrologia "G. Colonnetti" (IMGC), Torino, Italy, Physikalisch-Technische Bundesanstalt (PTB), Braunschweig, German Federal Republic, National Physical Laboratory (NPL), Teddington, United Kingdom, and the National Bureau of Standards (NBS), Gaithersburg, USA. The second phase included Bundesamt für Eich-und Vermessungswesen (BEV), Vienna, Austria, Československý Metrologický Ústav (CSMU), Bratislava, Czechoslovakia, Aeronautical Research Institute (FFA), Bromma, Sweden, and Office Federal de Metrologie (EAM), Wabern, Switzerland. The third phase included the National Research Laboratory of Metrology (NRLM), Ibaraki, Japan, the National Institute of Metrology (NIM) Beijing, China, Amt für Standardisierung, Messwesen und Warenprüfung (ASMU), Berlin, German Democratic Republic, and Gostandard-VNIIFTRI (VNIIFTRI), Moscow, Soviet Union. A fourth phase of the comparison is currently underway and

will include the standards of Hungary, South Africa, Denmark, and India.

The procedures and results of the first three phases of this comparison have been detailed in separate publications by the participants, and an overall summary is presented in references [1] and [2], which include references to the earlier reports. In brief, each participant determined the effective area of the transfer standard (the gravitational force of the piston and weights divided by the applied pressure as determined by the participant's standard) 17 times at 9 different pressures. The measured effective areas, $A(p)$, corrected to 20 °C, were then least-squares fitted to an equation of the form $A(p) = A_0 (1 + \lambda p)$. The zero-pressure effective area, A_0 , at 20 °C, and the distortion coefficient, λ , were then used to characterize each participant's results.

Repeated calibrations by the pilot laboratory of the transfer and backup gages indicated significant changes with time of the effective areas of the gages. It appears that the gages were asymptotically approaching a stable value, with the zero-pressure area of the transfer gage increasing from its initial value by 34 parts per million (ppm) over a 3-year period, and the backup gage's effective area increasing by 52 ppm over a period of 4 years. In order to account for this, the effective areas of the transfer gage, as determined by the pilot laboratory, were least-squares fitted to a seven parameter equation with time and pressure as the variables. Residuals from this equation were no greater than 3 ppm. This equation was used to calculate pilot-laboratory values of A_0 and λ appropriate to the time of each participants' measurements.

The differences between each participant's values of A_0 and λ , and the appropriate pilot-laboratory values, were combined in a weighted average to generate reference values of A_0 and λ . The inverse of the square of the uncertainty of each participant's results were used as weighting factors. The uncertainties included the reported systematic uncertainties of the participants standards, and three times the standard deviations of the fitted values of A_0 and λ obtained from the participant's results. The reference values were refined in an iterative series of calculations by excluding from the average all results that differed from the refined reference values by more than the uncertainty of the participants' results. In the end, the reference values for A_0 and λ each included the weighted results from 9 of the 13 participants.

Deviations between each participant's results and the reference values of A_0 are presented in reference [2] and similar results for λ and the effective area at 100 MPa (derived from A_0 and λ) are in references [1] and [2]. The results for A_0 , including the uncertainty of each participants results, are shown in figure 1.

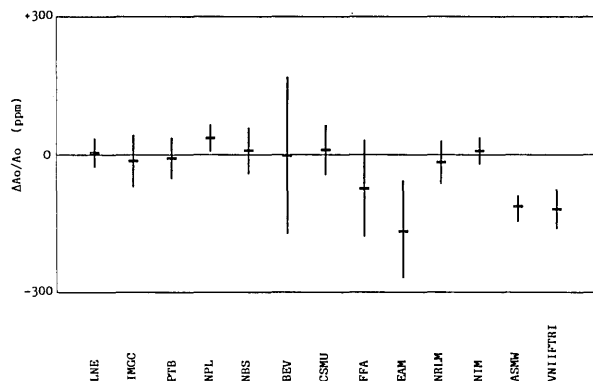


Figure 1. Fractional deviations of the zero pressure effective areas (A_0) determined by each participant from a weighted mean reference value. The error bars represent the uncertainties of the measured differences, including the uncertainty of the participants' standards, the uncertainty of the weights and thermometer used with the transfer standard, and three times the random uncertainty of the participants' determinations of A_0 . Figure obtained, with permission, from reference [2].

Barometric Pressures

The barometric or medium range pressures working group decided that its initial effort would be a comparison of absolute pressure standards between 10 and 110 kPa. NPL, Teddington, volunteered to act as pilot laboratory. Gas-operated piston gages, operating in the absolute mode, were selected as the transfer standards. Two piston and cylinder sets were provided by NBS. A special piston gage base, with provision for changing of weights while under vacuum, was provided by the National Measurement Laboratory (NML), Sydney, Australia. A thermometer, vacuum gage and pressure control system were provided by NPL.

Initial characterization of the transfer gage by NPL indicated significant instabilities. These were traced to an anodized aluminum finish on the piston assembly. Desorption of water from this surface under vacuum conditions, and reabsorption of water when exposed to atmospheric air, were causing large mass changes. This problem was eliminated by stripping the anodization and replacing it with a nickel coating. Subsequent repeated calibra-

tion of the gage by NPL at each of 10 different pressures had a mean standard deviation of 0.08 Pa.

Eighteen different laboratories have expressed a desire to participate in this comparison. The first phase of this comparison involved NPL, BIPM, and the Institut National de Metrologie (INM), Paris, France. In all cases the primary standards were mercury manometers. Agreement between the three laboratories was ± 0.5 Pa throughout the range, and none of the laboratories disagreed outside of their combined three sigma uncertainties.

Results are not yet available from a second phase, which will include CSMU, NML, and NBS. Further participation will be limited to laboratories that maintain independent primary standards, i.e., those whose standards are not traceable to the pressure standards of another laboratory.

The working group has proposed a further comparison of gage mode standards in the range 0.1 to 1 MPa. Eight laboratories have expressed an interest in participating in this comparison. However, no one has yet offered to act as pilot laboratory.

Low Pressures

After an initial discussion of comparing low range differential pressure standards, the low pressure working group decided on a comparison of absolute pressure standards. NBS volunteered to act as the pilot laboratory, using a high resolution mercury manometer as the reference standard. Since the working group did not know of previous interlaboratory comparisons in this range, there was only limited experience to guide the selection of transfer standards. After discussing and evaluating several alternatives, the working group selected capacitance diaphragm gages. These electromechanical transducers have adequate precision for this pressure range and the laboratories likely to participate are familiar with their use since they are often calibrated for industrial calibration customers. However, their response in the lower part of the range is complicated by thermal transpiration effects, and their long-term stability had not been well established.

Four gages were available for the comparison, two provided by NBS and one each by two manufacturers. Two gages with a 10 Torr (1333 Pa) range were selected to provide coverage of the entire range of the comparison, and two with a 1 Torr (133 Pa) range to give better precision at the low end of the range. After initial calibration by the pilot laboratory, calibration by the first participant, NPL, Teddington, and recalibration by the

pilot laboratory, it was evident that large shifts had occurred in some of the gages. Subsequent recalibration at the pilot laboratory showed further instabilities, even under laboratory conditions, with random magnitudes and direction. A second set of measurements was then made by NPL. The following calibration by the pilot laboratory showed smaller but still significant shifts in the gages. The decision was then made to suspend the comparison until the gage instabilities could be further evaluated.

By this time data were becoming available on the recalibration of similar gages used by industrial standards laboratories. These data indicated large differences in the stability level of different gages. The instabilities observed for the transfer gages are consistent with the instabilities observed for the industrial gages [3]. The results of continued recalibration of the transfer gages are shown in figure 2 and indicate that the magnitude of the shifts have decreased with time, particularly for one type of gage (B).

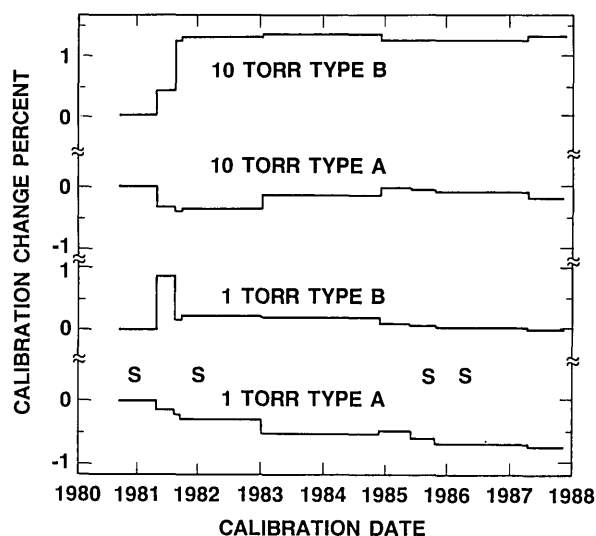


Figure 2. Changes with time of the calibration constants of the four transfer gages used for the low pressure comparison. The "S" marks the times when the gages were shipped overseas and back.

The encouraging decrease in gage instabilities prompted a resumption of the comparisons. In 1985–87 measurements were made by PTB, Berlin and NML. Subsequent calibration by the pilot laboratory showed changes in the transfer gages that, while larger than desirable, were significantly reduced from the earlier experience. Results are currently being evaluated.

Very Low Pressures

The very low pressure working group decided on a comparison with both argon and hydrogen. Argon is a widely used calibration gas, and hydrogen is an important gas for very low pressure metrology that presents special problems. PTB, Berlin, volunteered to be the pilot laboratory. The selection of a transfer gage was of some concern. Even under the best of circumstances, the widely used ionization gage is known to exhibit instabilities comparable to or larger than the uncertainties of primary standards. A possible alternative was a molecular drag gage. This gage measures pressures using the rotational decay rate of a magnetically suspended spinning ball (steel bearing ball) caused by collisions with gas molecules. This gage had only recently become available for routine laboratory use and only limited data were available on its stability, although these data were encouraging. In addition, the calibration of the gage is believed to depend only on the ball and the small gage tube containing the ball. Thus, only these small parts would have to be shipped to laboratories already possessing the gage electronics. Therefore, the decision was made to use the molecular drag gage; Kernforschungsanlage (KFA), Jülich, which was developing prototypes of the molecular drag gage for commercial production, made two electronic control units available for the intercomparison.

The working group developed a protocol involving a series of calibrations at specified pressures between 5×10^{-4} and 1 Pa. The pilot laboratory monitored the performance of the transfer gages before and after the measurements of each participant. For the initial participants, LNE, IMGC, NPL (Teddington), and CSMU, the transfer gages were hand-carried between laboratories, all of which were within a relatively short distance of the pilot laboratory. Measurements at the pilot laboratory indicated changes in the transfer gages of less than $\pm 0.4\%$ for any comparison. Larger changes were detected after measurements by the next two participants, NIM and NPL, New Delhi, India. In these cases the gages were also hand carried, but over much greater distances. Finally, after shipment by parcel post to and from NBS, the gages showed very large changes, as large as -8% for the hydrogen calibration of one gage.

The performance of the transfer gages and preliminary results of the comparisons, using argon, are detailed in reference [4]. It is believed that the cause of the instabilities is understood. The calibration factor of the molecular drag gage depends di-

rectly on the momentum transfer between gas molecules and the ball's surface. It was believed that the surfaces could be stabilized by deliberately roughening them using an acid etch, and shipping the balls under vacuum in the stainless steel gage tubes. It now appears that the surfaces of the roughened balls were polished as they rolled around in the stainless steel tubes during transport, with increasing changes in the gage constant as the distance and violence of the transport increased.

Subsequently, two new sets of four balls were characterized by the pilot laboratory and shipped to NBS, NPL (Teddington), and the Electro Technical Laboratory (ETL), Ibaraki, Japan. In this case the balls were restrained within the stainless steel tubes to minimize motion and the stability of the transfer gages have been satisfactory. The available calibration results for argon and hydrogen are shown in figure 3, and a final report is under discussion.

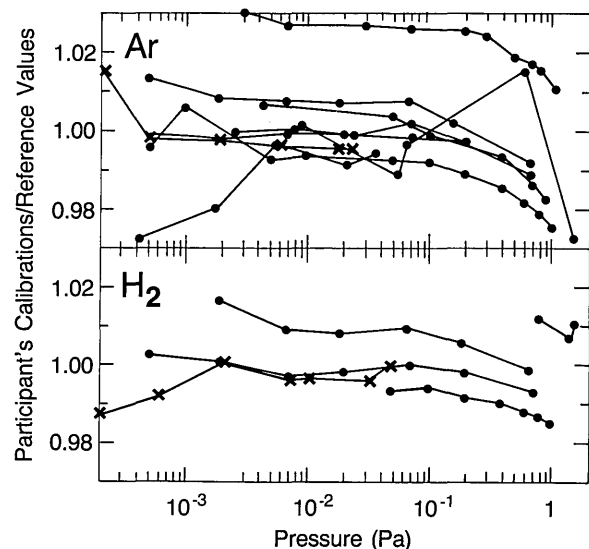


Figure 3. Preliminary results from seven of the participants in the very low pressure comparison, shown as dots, adapted from reference [4], with permission, with the second set of the results for NBS added as X's. The values plotted are the average ratios, for the four transfer gages, of the gage calibration constant determined by the participants to the reference value determined by the pilot laboratory.

Acknowledgment

The cooperation of Drs. Molinar (IMGC), Stuart (NPL, Teddington), and Messer and Jitschin (PTB) in providing material for this report is gratefully acknowledged.

About the author: Charles R. Tilford is a physicist in the Temperature and Pressure Division of the NBS Center for Basic Standards.

References

- [1] Molinar, G. F., Legras, J. C., Bean, V. E., Borovkov, V. M., Jager, J., Kepert, A., Lewis, S. L., Lewisch, R., Mobius, Rydstrom, L., Ulrich, J. G., Yamamoto, S., and Yi-tang, S., International Comparison of Pressure Measurements in a Liquid Medium from 20 to 100 MPa, Proceedings of the XI AIRAPT Conference, Kiev, July 1987.
- [2] Legras, J. C., Lewis, S. L., and Molinar, G. F., International Comparison in the Pressure Range 20–100 MPa, to be published in *Metrologia*.
- [3] Hyland, Richard W., and Tilford, Charles R., *J. Vac. Sci. Technol.* A3, 1731 (1985).
- [4] Messer, G., Röhl, P., Grosse, G., and Jitschin, W., *J. Vac. Sci. Technol.* A5, 2440 (1987).

Condensation Method for Humidity Measurement in the UMR Cloud Simulation Chamber

Volume 93

Number 4

July–August 1988

**D. E. Hagen, D. R. White,
and D. J. Alofs**

University of Missouri-Rolla
Rolla, MO 65401

The University of Missouri-Rolla has developed a cloud simulation facility for the study of various atmospheric cloud processes. The initial relative humidity of the air sample put into the cloud chamber is a key parameter in virtually any experiment and needs to be known accurately. This report describes how the cloud simulation chamber itself has been used as a condensation type hygrometer to calibrate the system's humidifier. Two distinct and physically different methods for inferring mixing ratio are used, one exploiting the sensi-

tivity of aerosol activation to humidity, and the other exploiting the sensitivity of the rate of growth of cloud droplets to humidity. The two methods give agreement with each other to within a precision of one part per thousand in mixing ratio.

Key words: aerosol activation; cloud drop growth; expansion cloud chamber; humidity measurement; mixing ratio; water vapor.

Accepted: February 17, 1988

1. Introduction

Several countries have developed facilities for accurately measuring humidity. Such a national facility ideally includes both an ultra stable humidity generator, and a primary standard for measuring relative humidity. The primary standard is used to calibrate the humidity generator, and the humidity generator is used to calibrate other portable instruments which have been sent to the national facility for calibration. The gravimetric hygrometer described by Wexler and Hyland [1] utilizes absorption of water vapor by a solid desiccant, and precision weighing of the absorbed water. The uncertainty is about plus or minus one part in a thousand for the measurement of mixing ratio (mass of water vapor per unit mass of dry gas). Gravimetric hygrometers are currently the primary standards in the United States [2], in Japan [3] and in the United Kingdom [4]. A chilled mirror condensation hygrometer [5] is utilized in France as a transfer hu-

midity standard. This instrument is periodically calibrated at the National Bureau of Standards in the United States and then returned to France for use as a standard in France. The accuracy is about plus and minus 0.03 °C in dew point. This corresponds to an uncertainty in mixing ratio of plus or minus 2 parts per thousand, or twice that of the gravimetric hygrometer. The chilled mirror hygrometer however, has the great advantage of portability.

The University of Missouri at Rolla has developed a cloud simulation facility for studying the processes that occur in clouds in the atmosphere. Part of the facility is a humidifier, which has an air flow rate of 1 L/s, and which produces relative humidities close to 100% at temperatures which can be set to within 0.01 °C over the range 5 to 25 °C [6]. Another part of the facility is a cooled wall expansion cloud chamber, which produces a

supersaturated environment so that water droplets can be grown on a sample of cloud condensation nuclei (CCN). A third part of the facility is the optical system used to observe the Mie scattering from the water droplets, thus determining the mean size of growing water droplets as a function of time. A fourth part of the facility is the aerosol generation system, used to supply the CCN sample to the simulation chamber. The cloud chamber, optical system, and aerosol generation system, and other components have been described by White et al. [6].

This report describes how the cloud simulation chamber has been used as a condensation type hygrometer to calibrate the humidifier with a precision of one part per thousand in mixing ratio. An error analysis to determine whether the absolute accuracy is as good as the precision has not been made. Since an error analysis for the gravimetric hygrometer has been made [1], there is more confidence in the absolute accuracy of the gravimetric hygrometer than in our facility. It would therefore be desirable to intercompare a gravimetric hygrometer to our facility, but this direct intercomparison wouldn't be feasible since neither facility is portable. It would be feasible to compare our humidity measurement technique to a portable hygrometer such as the chilled mirror instrument described by Merigourx and Cretinon [5] and our Center would welcome such an opportunity.

2. Expected Humidity from Humidifier

The humidifier consists of two columns each with 60 vertical glass rods, 0.7 cm diameter, spaced on alternate points of a 1.27-cm grid, and enclosed in an aluminum cylinder 16.5 cm inside diameter. Water flows downward on the glass surfaces, and air flows downward in the space between the glass rods. The two humidifier columns, each with an effective length of 89 cm, are connected in series with respect to the air flow. Thus the length of the humidifier is in effect 178 cm. The air flow rate is 1.0 L/s, and the water flow rate is 0.25 L/s.

The first concern addressed was whether the glass rods were isothermal over their length. As water evaporates at the rod surface the rods are cooled due to the latent heat absorbed. To calculate the amount of cooling an energy balance is performed. To humidify originally dry air the latent heat flux is 35.6 watts. This heat when supplied by the 0.25 L/s liquid water flow produces only a

0.034 °C temperature drop in the water. Thus the glass rods have essentially no axial temperature gradients.

The next concern is how to model the vapor diffusion in the humidifier. The problem is three dimensional, and would need to be solved numerically if one wished an accurate analysis. Instead a crude analysis was performed in which the three dimensional problem is approximated as a two dimensional problem for which an analytical solution exists. Specifically, the humidifier is modeled as a round tube, having the same hydraulic diameter as the cross section of the humidifier. The air velocity in the model tube equals the average air velocity in the actual humidifier (5.25 cm/s), and the length of the model tube equals the total length of the two humidifier columns (178 cm). The wall of the model tube is wet and isothermal. The air enters the model tube dry and at the wall temperature. The outlet relative humidity from the model tube is sought.

The solution to the above idealization of the vapor diffusion in the humidifier has been given by Shah [7]. The hydraulic diameter is $4A/P$, where A is the cross sectional area of the flow and P is the perimeter wetted by the flow. Applied to the humidifier, A is the area of a 16.5 cm circle minus the area of 60 circles of 0.7 cm diameter. P is the circumference of 60 circles 0.7 cm diameter. This gives a hydraulic diameter of 5.66 cm. The Reynolds number based on a 5.66 cm length and an air velocity of 5.25 cm/s is about 200, so the air flow is laminar. The Peclet number is about 115, so that vapor diffusion in the flow direction is small compared to that in the transverse direction. The 178 cm length divided by the 5.66 cm length and by the Peclet number is a nondimensional quantity called x^* by Shah. The mean outlet relative humidity, called $(1-\theta_m)$ in Shah's analysis, is a function of only x^* . For our x^* (0.272) the predicted mean outlet relative humidity is 98.45%, equivalent to a mean outlet dew point lower than the wall temperature by 0.256 °C. This result should be treated as a crude estimate. The resulting predicted dew point deficit of 0.256 °C is an order of magnitude estimate. It turns out that the observed humidity deficit is 0.29 °C, so the agreement is better than one could reasonably expect. Shah also gives an analytical solution for the equivalent diffusion problem between parallel plates. If the humidifier is evaluated in terms of equivalent parallel plates, the predicted dew point deficit is about an order of magnitude smaller (i.e., about 0.03 °C).

3. Humidity Measurement in the UMR Cloud Simulation Chamber

The initial relative humidity in the chamber, prior to expansion, is a key parameter in virtually any experiment. Despite the care that has gone into sample humidification, this has proved to be a difficult parameter to fix experimentally, and we have had to enlist additional means over and above the humidifier analysis given above in order to infer the humidity's value.

Two distinct and novel methods of inferring the initial mixing ratio from Mie scattering on a monodispersed cloud are described below. These have proved sufficiently accurate and reliable that we have adopted them in all subsequent experiments. The variable chosen to represent the initial water vapor content is mixing ratio, i.e., the number of grams of water vapor per gram of dry air and is denoted by r_0 .

3.1 Experiment Description

The experiment begins with a moist aerosol laden air sample at temperature T_0 and pressure p_0 . Usually T_0 is near 20 °C and p_0 is near 14.1 psi. The aerosol consists of NaCl particles of size near 0.025 μm radius and concentration near 100/cm³. The sample's initial relative humidity is typically near 83%. It is lowered below 100% by immediately raising the sample's temperature after it leaves the humidifier to avoid condensation loss of vapor (see [6]). At a relative humidity of 83%, the aerosol particles consist of very small ($\sim 0.05 \mu\text{m}$) solution droplets instead of dry particles. The sample is expanded to give a cooling rate of 10 °C/min, and the resulting cloud is observed via Mie scattering of laser light to determine drop size as a function of time. The aerosol exerts a negligible influence on the measurements of interest here. At our smallest observable drop size, 0.70 μm , a 10% change in the NaCl particle mass would only change the solution drop's equilibrium supersaturation ratio by 0.000006; an amount negligible in comparison to unity. Small variations in the critical supersaturation of the aerosol would have no appreciable effect on droplet growth rates.

3.2 Multiple Droplet Growth Rate Method

The condensational growth of water droplets is quite sensitive to humidity. Hence droplet growth rates can be used to give a measure of the air's water vapor content. In our method we take a

small set of droplet growth rate data containing at least two growth rate measurements and covering a short period of time. This data set is analyzed using drop growth theory to extract two unknowns, mixing ratio and sticking coefficient (β). A whole experiment can be subdivided into numerous small data sets, and a separate determination of r_0 made for each one. In each case the amount of water converted into the liquid state is accounted for in the determination of initial (before expansion) mixing ratio r_0 . r_0 should of course be constant.

The droplet growth rate equation [8] for the i -th droplet growth rate measurement can be written

$$r_0 = \epsilon / [p_i e_s(T_i)^{-1} \{ (a_i + 1) \dot{a}_i / D_{\text{eff}} \rho_{\text{sat}, i} + S_i^* \}^{-1} - 1]^{-1} + (4/3) \pi N a_i^3, \quad (1)$$

with $\epsilon = 0.62197$, p is the total pressure, N is the droplet concentration per gram of dry air, e_s is water saturation vapor pressure, T is absolute temperature, a is the droplet radius, \dot{a} is the droplet growth rate, D_{eff} is an effective diffusion coefficient (see [9]) for water vapor in air, ρ_{sat} is the saturation water vapor density over a flat surface, S^* is the equilibrium supersaturation ratio over a droplet of radius a , and

$$1 = D_{\text{eff}} (1_\alpha L B / K R_v T + 1_\beta / D), \quad (2)$$

$$1_\alpha = (1 - \alpha/2) K (\gamma - 1) (8\pi T / R_a)^{1/2} [\alpha p (\gamma + 1)]^{-1}, \quad (3)$$

$$1_\beta = (1/\beta - 1/2) D (2\pi / R_v T)^{1/2}. \quad (4)$$

Here D is the diffusion coefficient for water vapor in air, L is the latent heat of condensation for water, B is the slope of the e_s vs temperature curve, K is the thermal conductivity of moist air, R_v is the gas constant for water vapor, R_a is the gas constant for dry air, α is the thermal accommodation coefficient (here we use $\alpha = 1$), and γ is the specific heat ratio of moist air. The amount of water in the system is constant, so eq (1) should have the same value for all drop growth rate measurement points. This fact can be used to eliminate the unknown β . Define a minimization parameter as:

$$\chi^2 = \frac{\sum_{i=1}^I \sum_{j=1}^{i-1} (r_{0i} - r_{0j})^2 / [\delta(r_{0i} - r_{0j})]^2}{\sum_{ij} [\delta(r_{0i} - r_{0j})]^{-2}}, \quad (5)$$

where $\delta(r_{0i} - r_{0j})$ denotes the uncertainty in the knowledge of $r_{0i} - r_{0j}$. This uncertainty is calculated

based on a $0.05 \mu\text{m}$ uncertainty in a , a 20% uncertainty in \dot{a} , and a 5% uncertainty in N . The condensation coefficient enters into χ^2 through l . Since r_0 is constant χ^2 should be zero or at least small. Using the computer routine STEPIT, β can be varied to minimize χ^2 . This yields a value for β which can be put back into eq (1) to get r_0 . This process can be repeated for each data subset taken during the experiment to give multiple measurements of the same quantity r_0 .

3.3 Cloud Arrival Time Method

During a given expansion, the cloud is observable soon after saturation (100% relative humidity) is reached, and this observation provides a good determination of the saturation event. The cloud droplets can be observed starting at $0.70 \mu\text{m}$ radius. The small time increment, on the order of one second, between saturation and first cloud observation, can be accounted for by droplet growth modeling. For the special case of expansions using constant cooling rates (temperature is a linear function of time), this time increment is very insensitive to r_0 . The method simply involves observing the cloud arrival time, subtracting the above time increment from this to determine the time at which the gas sample reached 100% relative humidity, noting the gas temperature and pressure at this time (100% relative humidity), and finally calculating the mixing ratio r_0 of the gas from this information.

This method is only applicable to experiments using constant cooling rates which make the above time increment independent of r_0 . Also the method is applied only to experiments using monodispersed CCN aerosols and fairly fast expansion rates. These conditions lead to monodisperse clouds (all drops are the same size), and allow the use of Mie scattering of laser light as the drop sizing method [6].

The time increment between the 100% relative humidity point and the cloud first observation point is calculated from droplet growth theory, and does depend on the sticking coefficient. However this particular situation involves freshly produced droplets, and fresh water surfaces are thought to have large sticking coefficients near unity [10]. The sticking coefficient results taken from the droplet growth rate method described above confirm this for the early stage of the cloud's lifetime. Hence, in the time increment calculation, a sticking coefficient of unity is assumed. The influence of sticking coefficient is modest here in any case. A change in sticking coefficient by a factor of

2 (or 5) leads to a change in r_0 by an amount 0.000006 (or 0.000023).

The cloud arrival time method hasn't been optimized and therefore improvements could be achieved. For instance, the influence of the sticking coefficient could be minimized by choosing a slower expansion rate and a more sharply monodispersed CCN aerosol. This would reduce the change in temperature, pressure, and humidity during the time interval during which the cloud drops grew to observable size.

3.4 Numerical Cloud Model Tests

As discussed above, a numerical cloud model, which calculates gas thermodynamics and water droplet growth processes, is used in this analysis. For this we use the numerical model presented by Hagen [9]. This model has been successfully tested against older results in the literature [9] and against the NASA Analytic Simulator [11,12]. Anderson, Hallett, and Beesley [13] presented an extended solution to the droplet growth problem and gave an intercomparison among the leading droplet theories. They conclude that Carsten's [8] solution of the droplet growth problem is quite adequate. This is the solution on which our cloud model is based. Furthermore Anderson et al. [13] presented numerical results from their extended model for numerous test cases. We calculated these cases with our model and agreed with their results to within 2% for drop size.

4. Results

The experimental results from five different days of work are given in table 1. The run number gives a unique identification number for each experiment. The first six digits of the run number give the date (month-day-year) on which the experiment was performed. These experiments run from September 1986 to November 1987. The column labeled $r_0(\text{MDG})$ gives the values for the mixing ratio obtained from the multiple drop growth rate method. This represents the average of repeated measurements of this quantity during the course of the experiment. Since r_0 represents the initial value of the mixing ratio, it is fixed and all of these repeated measurements should yield the same value. $\sigma(\text{MGR})$ denotes the standard deviation of the individual results around the average and is a measure of experiment consistency. Note that $\sigma(\text{MGR})$

Table 1. Numerical cloud model tests

Run	$r_0(\text{MGR})$	$\sigma(\text{MGR})$	$r_0(\text{CAT})$	Δr_0
091086.04	0.012582	0.000008	0.012591	0.000009
091086.05	0.012574	0.000012	0.012550	-0.000024
091086.06	0.012580	0.000022	0.012570	-0.000010
091086.07	0.012605	0.000005	0.012615	0.000010
111886.A1	0.012618	0.000010	0.012630	0.000012
111886.A3	0.012733	0.000007	0.012752	0.000019
111886.A4	0.012551	0.000010	0.012565	0.000014
121786.01	0.012480	0.000005	0.012488	0.000008
121786.02	0.012483	0.000007	0.012485	0.000002
121786.03	0.012503	0.000006	0.012512	0.000009
121786.04	0.012521	0.000013	0.012533	0.000012
121786.05	0.012509	0.000006	0.012519	0.000010
121786.06	0.012520	0.000008	0.012524	0.000004
121786.07	0.012530	0.000011	0.012526	-0.000004
121786.08	0.012523	0.000008	0.012541	0.000018
121786.09	0.012525	0.000012	0.012523	-0.000002
121786.10	0.012528	0.000045	0.012524	-0.000004
080787.01	0.012668	0.000018	0.012689	0.000021
100687.01	0.012510	0.000008	0.012506	-0.000004

is usually small, indicating good consistency between the various measurements taken in a given run. $r_0(\text{CAT})$ denotes the initial mixing ratio as determined by the cloud arrival time method. Δr_0 denotes the difference between the two methods, i.e., $\Delta r_0 = r_0(\text{CAT}) - r_0(\text{MGR})$.

The average of the absolute difference between $r_0(\text{MDG})$ and $r_0(\text{CAT})$ is 0.000010, with standard deviation around the average of 0.000007. This average difference between the two methods corresponds to a difference of 0.012 °C in dew point. Hence the two methods are in good agreement with each other. The average difference between measured humidifier temperature and dew point is 0.29 °C, corresponding to a relative humidity of 98.1% for the air coming from the humidifier. This figure is in agreement with the rough estimate of expected humidifier performance under these conditions (0.26 °C difference between humidifier temperature and dew point, or 98.45% relative humidity for air leaving the humidifier) that was given above.

5. Conclusion

The problem of determining the water vapor content of gas sample is addressed using the condensational growth of airborne water droplets as the measurement tool. Two distinct methods are employed. One is based on multiple measurements of droplet growth rate; the other is based on the

fact that cloud is observable almost immediately after the gas sample is brought through 100% relative humidity. These two quite different methods give good agreement with each other. The average difference in calculated initial mixing ratio is 0.000010 grams of water per gram of dry air (corresponding to about 8 parts in 10^4), with a standard deviation of 0.000007 gram/gram-air. This corresponds to a dew point difference of 0.012 °C. This agreement gives us substantial confidence in our determination of water vapor content.

6. Acknowledgment

This work was supported by the Office of Naval Research (ONR N00014-75; ONR N00014-75-C-0413; ONR N00014-75-C-1152), Air Force Office of Scientific Research (Tri-service funded by ONR, AFOSR, and ARO: AFOSR F49620-80-C-0090; AFOSR 850071), Army Research Office (DAAK 70-C-0241).

About the authors: D. E. Hagen is with the Department of Physics, University of Missouri-Rolla, D. R. White is with the Department of Engineering Mechanics, University of Missouri-Rolla, and D. J. Alofs is a member of the Department of Mechanical Engineering and Graduate Center for Cloud Physics Research, University of Missouri-Rolla.

References

- [1] Wexler, A., and Hyland, R. W., The NBS standard hygrometer. In Humidity and Moisture, Wexler, ed., Vol. III, Reinhold Publ. (1965).
- [2] Hasegawa, S., National basis of accuracy in humidity measurements. In Moisture and Humidity, Instrument Society of America, Proc. 1985 Int. Symp. on Moisture and Humidity, Washington, DC, April 1985, pp. 15–28.
- [3] Takahashi, C., and Inamatsu, T., Construction of a gravimetric hygrometer. In Moisture and Humidity, Instrument Society of America, Proc. 1985 Int. Symp. on Moisture and Humidity, Washington, DC, April 1985, pp. 91–100.
- [4] Forton, A. G., and Pragnell, R. F., Development of the primary gravimetric hygrometer for the U.K. national humidity standard facility. In Moisture and Humidity, Instrument Society of America, Proc. 1985 Int. Symp. on Moisture and Humidity, Washington, DC, April 1985, pp. 79–89.
- [5] Merigoux, J., and Cretinon, B., A transfer humidity standard for dew point temperatures in the range from -20 °C and +60 °C. In Moisture and Humidity, Instrument Society of America, Proc. 1985 Int. Symp. on Moisture and Humidity, Washington, DC, April 1985, pp. 401–410.

- [6] White, D. R., Kassner, J. L., Carstens, J. C., Hagen, D. E., Schmitt, J. L., Alofs, D. J., Hopkins, A. R., Trueblood, M. B., Alcorn, M. W., and Walker, W. L., *Rev. Sci. Instrum.* **58**, 826 (1987).
- [7] Shah, R. K., Thermal entry length solutions for the circular tube and parallel plates. *Proc. 3rd Natl. Heat Mass Transfer Conf., Indian Institute of Technol., Bombay, Vol. I, Paper No. HMT-11-75* (1975).
- [8] Carstens, J. C., *Adv. Colloid Interface Sci.* **10**, 285 (1979).
- [9] Hagen, D. E., *J. Appl. Meteor.* **18**, 1035 (1979).
- [10] Pruppacher, H. R., and Klett, J. D., *Microphysics of clouds and precipitation*. D. Reidel, Boston (1978).
- [11] Plooster, M., Atmospheric cloud physics laboratory simulation system; mathematical description. Report under NASA contract NAS8-32668 (1979).
- [12] Plooster, M., Atmospheric cloud physics laboratory simulation system; users guide. Report under contract NAS8-32668 (1979).
- [13] Anderson, B. J., Hallett, J., and Beesley, M., An extended classical solution of the droplet growth problem. NTIS #NASA TM-82392 (1981).

Precipitation of $NH_4UO_2PO_4 \cdot 3H_2O$ — Solubility and Structural Comparison with Alkali Uranyl(2+) Phosphates

Volume 93

Number 4

July–August 1988

Milenko Marković¹

“Rudjer Bošković” Institute,
Zagreb, Yugoslavia and
ADAHF,
National Bureau of Standards
Gaithersburg, MD 20899

Nevenka Pavković

Faculty of Science,
Zagreb, Yugoslavia

and

Neven D. Pavković

“Rade Končar” Selfmanagement
Corporation, Zagreb, Yugoslavia

Precipitates formed in the system $UO_2(NO_3)_2 \cdot NH_4OH \cdot H_3PO_4 \cdot H_2O$, aged for 30 days at 298 K, were studied. The precipitates were characterized by chemical and thermogravimetric analyses, x-ray powder diffraction, infrared spectroscopy, polarized light microscopy, and by their fluorescent properties. The precipitation boundary was established tindalometrically and microscopically. On the basis of these measurements, the stability conditions, structural parameters, and solubility of the tetragonal polymorph of $NH_4[UO_2PO_4] \cdot 3H_2O$ were determined. This compound shows a close structural relationship with $H_3O[UO_2PO_4] \cdot 3H_2O$ (space group $P4/ncc$) and alkali uranyl(2+) phosphates polyhydrates $M[UO_2PO_4] \cdot nH_2O$ ($n=4$ for $M=Li$; $n=3$ for $M=Na, K, Rb$ and $n=2.5$ for $M=Cs$). The unit-cell dimensions determined for $NH_4UO_2PO_4 \cdot 3H_2O$ are: $a=b=7.02 \text{ \AA}$, $c=18.08 \text{ \AA}$ ($P4/ncc$).

The thermodynamic solubility product constant, $K_s = a(NH_4^+) \times a(UO_2^{2+}) \times a(PO_4^{3-})$, for $NH_4UO_2PO_4 \cdot 3H_2O$ was determined: $\log K_s = -26.50 \pm 0.09$. The K_s values of $M[UO_2PO_4] \cdot nH_2O$ (at ionic strength, $I=0.23 \text{ mol dm}^{-3}$) calculated from previously published experimental data by using correct stability constants of uranyl(2+) phosphate complexes are: $\log K_s = -22.61 \pm 0.08$ for $M=Na$; $\log K_s = -23.92 \pm 0.12$ for $M=K$; $\log K_s = -24.13 \pm 0.19$ for $M=Rb$; $\log K_s = -23.80 \pm 0.20$ for $M=Cs$; and $\log K_s = -24.74 \pm 0.10$ for $M=NH_4$, showing that $NH_4UO_2PO_4 \cdot 3H_2O$ is less soluble than corresponding alkali uranyl(2+) phosphates.

Key words: alkali uranyl(2+) phosphates; ammonium uranyl(2+) phosphate; precipitation; solubility product; unit-cell dimensions; x-ray diffraction pattern.

Accepted: April 4, 1988

Introduction

The formation of uranyl(2+) phosphates ($UO_2HPO_4 \cdot 4H_2O$ and $(UO_2)_3(PO_4)_2 \cdot 8H_2O$) and alkali uranyl(2+) phosphates ($MUO_2PO_4 \cdot nH_2O$; $M=Li, Na, K, Rb, Cs$; $4 \geq n \geq 2.5$) by spontaneous precipitation from supersaturated solutions and the stability of uranyl phosphate complexes has been

described in some of our previous papers [1–5]. These compounds are important for the production of uranium from low-grade phosphate ores and in fuel reprocessing [6–8].

Precipitation conditions of ammonium uranyl(2+) phosphate can be of interest for the separation of uranium as a secondary product in the production of monoammonium phosphate (additive of fertilizers) [9]. Three polymorphs of $NH_4UO_2PO_4 \cdot 3H_2O(s)$ are known [10,11]. The solubility product of one of these compounds has been

¹ Author to whom correspondence should be addressed at Department of Physical Chemistry, “Rudjer Bošković” Institute, P.O. Box 1016, 41001 Zagreb, Yugoslavia or American Dental Association Health Foundation, Paffenbarger Research Center, National Bureau of Standards, Gaithersburg, MD 20899.

determined at undefined ionic strength [12,13] and at an ionic strength of 0.23 mol dm^{-3} [14] using inaccurate association and stability constants for phosphoric acid and uranyl phosphate complexes, respectively.

This paper describes the formation of different precipitates in the system $\text{UO}_2(\text{NO}_3)_2\text{-NH}_4\text{OH-H}_3\text{PO}_4\text{-H}_2\text{O}$ at 298 K. These precipitates were characterized by chemical and physical methods. The stability region for the precipitated tetragonal polymorph of $\text{NH}_4\text{UO}_2\text{PO}_4\cdot 3\text{H}_2\text{O}$ was established as a function of reactant concentrations, and its solubility product constant was determined. The structure of this polymorph was compared to that of hydrogen uranyl(2+)phosphate [2,15] and alkali uranyl(2+)phosphates [3,4]. The solubility data for $\text{NH}_4\text{UO}_2\text{PO}_4\cdot 3\text{H}_2\text{O}$ and $\text{MUO}_2\text{PO}_4\cdot n\text{H}_2\text{O}$ obtained by Vesely, Pekarek, and Abbrent [14] were recalculated in this paper using a proper set of constants to obtain solubility products, and they were compared with our data.

Experimental Section

Stock solutions were prepared by dissolving the following P.A. chemicals in triply distilled water: $\text{UO}_2(\text{NO}_3)_2$, H_3PO_4 , and NH_4OH (Merck,² Darmstadt). Standardization of solutions was performed by using classical analytical methods [16,17].

Precipitation in the system $\text{UO}_2(\text{NO}_3)_2\text{-NH}_4\text{OH-H}_3\text{PO}_4\text{-H}_2\text{O}$ (at 298 K) was performed at constant uranyl(2+)nitrate concentration, $1 \times 10^{-3} \text{ mol dm}^{-3}$; the concentrations of NH_4OH varied from 5×10^{-5} to 3.2 mol dm^{-3} and phosphoric acid from 5×10^{-3} to 1 mol dm^{-3} . The samples were prepared by mixing $\text{UO}_2(\text{NO}_3)_2$ solution with an equal volume of $\text{NH}_4\text{OH} + \text{H}_3\text{PO}_4$ solution. Approximately 400 samples were prepared to define precipitation and phase boundaries. One day and 30 days after mixing the reactant solutions, the samples were examined in detail. The pH was measured with the Radiometer equipment: electrode GK 2302 C and pH-meter Mo 26. The precipitation boundary (the line that separates the region of precipitation from the region of clear solutions) was determined turbidimetrically and microscopically. The morphol-

ogy of the precipitates was examined in white, polarized and UV light under an Orthoplan microscope (Leitz, Wetzlar). Selected precipitates were characterized by means of chemical and thermogravimetric analyses (TGA), x-ray powder diffraction patterns (XRD) and infrared (IR) spectra. The phase boundaries (lines that separate the regions in which different solid phases precipitate) were determined on the basis of these data.

The solid phase was chemically analyzed for uranium, phosphorus and nitrogen. Uranium was precipitated with $(\text{NH}_4)_2\text{HPO}_4$, heated at 1373 K and weighed as $\text{U}_2\text{O}_3\text{P}_2\text{O}_7$ [18]. Phosphorus was determined gravimetrically by precipitation with ammonium molybdate [19] and spectrophotometrically as phosphovanadomolybdate complex [19]. Nitrogen was determined by chemical microanalysis. The water content was determined thermogravimetrically (Cahn RG recording electromicrobalance).

X-ray diffraction patterns were recorded on a Phillips x-ray diffractometer with a proportional counter, using graphite monochromated $\text{CuK}\alpha$ radiation. The x-ray patterns were calibrated with graphite as the internal standard [10] with a unit-cell $a = 2.463 \text{ \AA}$, $c = 6.714 \text{ \AA}$ ($\lambda = 1.54178 \text{ \AA}$). Relative intensities, I_{rel} , are given as peak heights. IR spectra (600 to 3600 cm^{-1}) were obtained using a Perkin-Elmer Mo-221 spectrophotometer and the standard KBr pellet technique.

Results

The concentration diagram of $\text{UO}_2(\text{NO}_3)_2\text{-NH}_4\text{OH-H}_3\text{PO}_4\text{-H}_2\text{O}$ systems aged for 30 days is presented in figure 1. The precipitation and phase boundaries (full lines) and iso-pH curves (dotted lines) are shown. Only the experimental points representing samples in which solid phase was fully examined (XRD, IR, TGA, chemical analysis) are shown in figure 1 (filled circles). Chemical and TG analyses revealed that the solid phase was $\text{NH}_4\text{UO}_2\text{PO}_4\cdot 3\text{H}_2\text{O}$:

	% U	% P	% N	% H ₂ O
Found:	54.28–54.60	7.06–7.12	3.16–3.25	12.30–12.40
Theoretical:	54.46	7.09	3.20	12.36

TGA showed the loss of $2.4 \pm 0.2 \text{ mol H}_2\text{O}$ up to 353 K and an additional $0.6 \pm 0.2 \text{ mol}$ loss in the interval from 353 to 403 K. Transformation of anhydrous $\text{NH}_4\text{UO}_2\text{PO}_4$ to UO_2HPO_4 (loss of NH_3) starts at 450 K. The IR spectrum of

² Certain commercial materials and equipment are identified in this paper to specify the experimental procedure. In no instance does such identification imply recommendation or endorsement by the National Bureau of Standards or the ADA Health Foundation or that the material or equipment identified is necessarily the best available for the purpose.

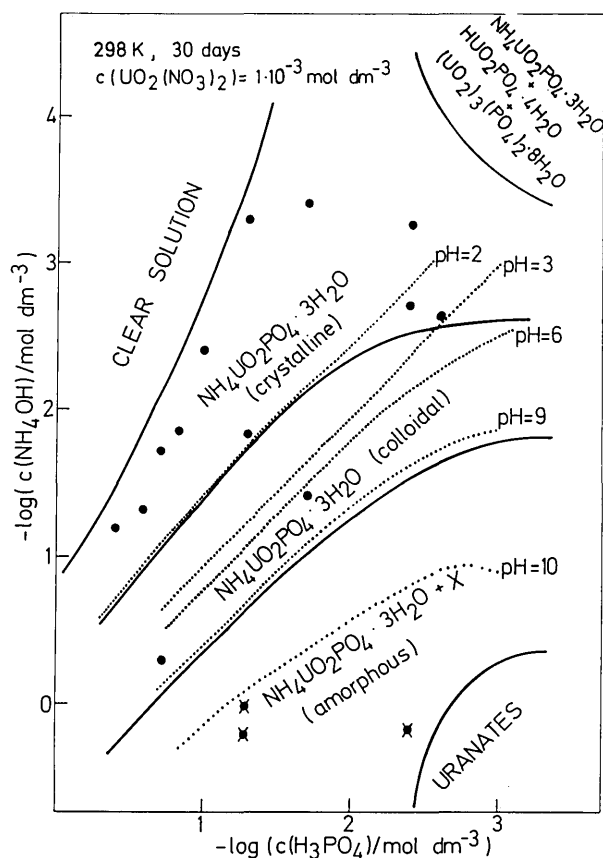


Figure 1. Precipitation diagram for the system $\text{UO}_2(\text{NO}_3)_2\text{-NH}_4\text{OH-H}_3\text{PO}_4\text{-H}_2\text{O}$ aged for 30 days. Precipitation and phase boundaries are denoted by full lines and iso-pH curves by dotted lines. In the samples (●, X), the solid phase was identified by XRD, IR, chemical, and TG analysis and found to be $\text{NH}_4\text{UO}_2\text{PO}_4\cdot 3\text{H}_2\text{O}$ (●) and an undefined compound (X).

$\text{NH}_4\text{UO}_2\text{PO}_4\cdot 3\text{H}_2\text{O}$ showed characteristic phosphate and uranyl vibrations [20].

In table 1 are given observed d -values (d_{obsd}) and the relative intensities (I_{rel}) for $\text{NH}_4\text{UO}_2\text{PO}_4\cdot 3\text{H}_2\text{O}$ obtained by XRD. Comparison of the x-ray powder pattern of $\text{NH}_4\text{UO}_2\text{PO}_4\cdot 3\text{H}_2\text{O}$ with those of the $\text{H}_3\text{O}[\text{UO}_2\text{PO}_4]\cdot 3\text{H}_2\text{O}$ [2,15] confirms a close structural relationship among them ($P4/ncc$ space group, structure: metatorbernite); the ($h00$) and ($00l$) reflections were used to calculate the unit cell parameters for $\text{NH}_4\text{UO}_2\text{PO}_4\cdot 3\text{H}_2\text{O}$: $a = b = 7.02(1)$ Å, and $c = 18.08(4)$ Å. The hkl indices and d_{calcd} values (table 1) are calculated on the basis of unit-cell parameters by using computer programs [21,22]. The excellent agreement between observed and calculated d values (table 1) indicate a pure tetragonal polymorph $\text{NH}_4\text{UO}_2\text{PO}_4\cdot 3\text{H}_2\text{O}$.

$\text{NH}_4\text{UO}_2\text{PO}_4\cdot 3\text{H}_2\text{O}$ crystallizes in the broad concentration range $\text{pH} \leq 2$ (fig. 1). Its crystals were in

Table 1. x-ray powder pattern for $\text{NH}_4\text{UO}_2\text{PO}_4\cdot 3\text{H}_2\text{O}$ ($P4/ncc$, $a = 7.02$ Å, $c = 18.08$ Å, $Z = 4$)

h	k	l	$d_{\text{obsd}}/\text{Å}$	$d_{\text{calcd}}/\text{Å}$	I_{rel}
0	0	2	9.08	9.04	100
1	0	2	5.56	5.54	20
1	1	0	4.97	4.96	12
0	0	4	4.53	4.52	12
1	1	2	4.35	4.35	14
1	0	4	3.80	3.80	51
2	0	0	3.51	3.51	17
1	1	4	3.34	3.34	1
2	0	2	3.28	3.27	20
2	1	1	3.09	3.09	1
0	0	6	3.02	3.01	1
2	1	2	2.97	2.97	9
2	1	3	2.78	2.78	29
2	1	4	2.58	2.58	8
2	2	0	2.48	2.48	4
2	2	2	2.39	2.39	5
3	0	2	2.27	2.27	14
3	1	0	2.22	2.22	6
3	1	1	2.21	2.20	3
2	2	4	2.18	2.18	12
3	1	2	2.16	2.16	15
3	1	3	2.08	2.08	6
3	0	4	2.07	2.08	3
1	1	8	2.06	2.06	9
2	1	7	1.998	1.995	1
2	0	8	1.901	1.900	4
3	0	6	1.849	1.848	4
2	1	8	1.834	1.834	5
0	0	10	1.808	1.808	5
3	2	4	1.788	1.788	4
4	0	0	1.754	1.755	1
1	0	10	1.751	1.751	1
4	0	2	1.723	1.723	1
1	1	10	1.699	1.699	12
4	1	1	1.695	1.695	6
2	2	8	1.672	1.671	1
3	3	0	1.655	1.655	1
4	0	4	1.636	1.636	4
3	0	8	1.626	1.626	3
2	0	10	1.608	1.607	6
4	1	4	1.595	1.593	2
3	1	8	1.585	1.584	4
4	2	0	1.570	1.570	1
4	2	2	1.547	1.547	1
0	0	12	1.508	1.507	2
4	2	4	1.484	1.483	1
3	2	8	1.475	1.475	3
2	2	10	1.462	1.461	2
1	1	12	1.442	1.442	6
4	2	5	1.439	1.440	3

the form of squarish platelets showing an intense green fluorescence. In the region where a small increase in the ratio $c(\text{NH}_4\text{OH})/c(\text{H}_3\text{PO}_4)$ (at constant $c(\text{H}_3\text{PO}_4)$) causes a steep jump in the pH values of successive samples (from 2 to 9), stable colloidal particles obtained. At low concentrations

of NH_4OH and H_3PO_4 mixtures of $\text{NH}_4\text{UO}_2\text{PO}_4 \cdot 3\text{H}_2\text{O}$ with $\text{H}_3\text{O}[\text{UO}_2\text{PO}_4] \cdot 3\text{H}_2\text{O}$ and $(\text{UO}_2)_3(\text{PO}_4)_2 \cdot 8\text{H}_2\text{O}$ were found. At $\text{pH} > 9$ mixtures of amorphous $\text{NH}_4\text{UO}_2\text{PO}_4 \cdot 3\text{H}_2\text{O}$ (prevailing solid phase) and an undefined compound (designated by X in fig. 1) precipitated. The chemical identification of X was not possible due to its extremely small presence (less than 5 %).

In table 2 are given the concentrations of all components in the solutions equilibrated with $\text{NH}_4\text{UO}_2\text{PO}_4 \cdot 3\text{H}_2\text{O}(\text{s})$ (points along the precipitation boundary). The ionic concentration product, $K_s = c(\text{NH}_4^+) \times c(\text{UO}_2^{2+}) \times c(\text{PO}_4^{3-})$, expressed in greater detail form is

$$K_s = \frac{c(\text{UO}_2)_{\text{soln}} \times c(\text{NH}_4)_{\text{soln}} \times c(\text{H}_3\text{PO}_4)}{K_{13} \times K_{12} \times K_1 \times a^3(\text{H}^+)} \\ \times \sum_{i=0} \sum_{j=0} \left(\frac{\beta_{ij} \times c(\text{H}_3\text{PO}_4)^{i+j}}{a(\text{H}^+)^j} \right)^{-1}$$

In this equation $c(\text{UO}_2)_{\text{soln}}$ and $c(\text{NH}_4)_{\text{soln}}$ are the total concentrations of uranyl and ammonium species in the solution, respectively. K_{13} , K_{12} , and K_1 are the association constants of phosphoric acid [23–25] (table 3, equilibria 1–3) and β_{ij} are the stability constants of different uranyl phosphate complexes [5] (table 3, equilibria 4–7). The calculations were performed using a computer program de-

Table 2. Equilibrium concentrations determined according to precipitation boundary^a and calculated K_s values for $\text{NH}_4\text{UO}_2\text{PO}_4 \cdot 3\text{H}_2\text{O}(\text{s})$

System no.	$10^2 \times c(\text{PO}_4)_{\text{soln}} / \text{mol dm}^{-3}$	$10^4 \times c(\text{NH}_4)_{\text{soln}} / \text{mol dm}^{-3}$	pH	$10^2 \times I / \text{mol dm}^{-3}$	$\log K_s$	$\log K_s(I=0)$
1	5.0	2.25	1.76	1.90	-26.03	-26.83
2	6.0	4.50	1.71	2.13	-25.84	-26.68
3	8.0	9.00	1.69	2.48	-25.63	-26.52
4	10.0	17.50	1.61	2.89	-25.52	-26.46
5	15.0	40.00	1.53	3.73	-25.40	-26.43
6	20.0	90.00	1.43	4.69	-25.27	-26.39
7	25.0	125.00	1.41	5.40	-25.24	-26.42
8	30.0	175.00	1.33	6.26	-25.26	-26.51
9	40.0	350.00	1.31	8.06	-25.09	-26.44
10	50.0	550.00	1.30	9.95	-24.99	-26.44
11	80.0	1250.00	1.23	15.88	-24.89	-26.54

^a In all systems $c(\text{UO}_2)_{\text{soln}} = 1 \times 10^{-3} \text{ mol dm}^{-3}$.

Table 3. Homogeneous and heterogeneous equilibria^a

	$\log K(I=0)$	Ref.	$\log K(I=0.23 \text{ mol dm}^{-3})$	Ref.
1. $\text{H}_2\text{PO}_4^- + \text{H}^+ = \text{H}_3\text{PO}_4$	2.148 (K_{13})	23	2.01	23 ^c
2. $\text{HPO}_4^{2-} + \text{H}^+ = \text{H}_2\text{PO}_4^-$	7.199 (K_{12})	24	6.77	24 ^c
3. $\text{PO}_4^{3-} + \text{H}^+ = \text{HPO}_4^{2-}$	12.35 (K_1)	25	11.64	25 ^c
4. $\text{UO}_2^{2+} + \text{H}_3\text{PO}_4 = \text{UO}_2\text{H}_2\text{PO}_4^+ + \text{H}^+$	1.50 (β_{01})	5	1.28	5 ^o
5. $\text{UO}_2^{2+} + \text{H}_3\text{PO}_4 = \text{UO}_2\text{H}_3\text{PO}_4^{2+}$	1.30 (β_{10})	5	1.30	5 ^c
6. $\text{UO}_2^{2+} + 2\text{H}_3\text{PO}_4 = \text{UO}_2(\text{H}_2\text{PO}_4)_2^0 + 2\text{H}^+$	1.30 (β_{02})	5	0.93	5 ^c
7. $\text{UO}_2^{2+} + 3\text{H}_3\text{PO}_4 = \text{UO}_2(\text{H}_3\text{PO}_4)(\text{H}_2\text{PO}_4)_2^0 + 2\text{H}^+$	2.30 (β_{12})	5	1.93	5 ^c
8. $\text{H}^+ + \text{OH}^- = \text{H}_2\text{O}$	13.997 (K_w)	25	13.86	25 ^c
9. $\text{NH}_4\text{UO}_2\text{PO}_4 \cdot 3\text{H}_2\text{O}(\text{s}) = \text{NH}_4^+ + \text{UO}_2^{2+} + \text{PO}_4^{3-}$	$\begin{cases} -26.50 \pm 0.09 \\ -26.52 \end{cases}$	$\begin{cases} \text{b} \\ \text{c,f} \end{cases}$	$\begin{cases} -24.74 \pm 0.10 \\ -24.72 \end{cases}$	$\begin{cases} \text{c} \\ \text{b,e} \end{cases}$
10. $\text{NaUO}_2\text{PO}_4 \cdot 3\text{H}_2\text{O}(\text{s}) = \text{Na}^+ + \text{UO}_2^{2+} + \text{PO}_4^{3-}$	-24.39	c,f	-22.61 \pm 0.08	c
11. $\text{KUO}_2\text{PO}_4 \cdot 3\text{H}_2\text{O}(\text{s}) = \text{K}^+ + \text{UO}_2^{2+} + \text{PO}_4^{3-}$	$\begin{cases} -25.78 \pm 0.28 \\ -25.70 \end{cases}$	$\begin{cases} \text{d} \\ \text{c,f} \end{cases}$	$\begin{cases} -23.92 \pm 0.12 \\ -23.99 \end{cases}$	$\begin{cases} \text{c} \\ \text{d,e} \end{cases}$
12. $\text{RbUO}_2\text{PO}_4 \cdot 3\text{H}_2\text{O}(\text{s}) = \text{Rb}^+ + \text{UO}_2^{2+} + \text{PO}_4^{3-}$	-25.91	c,f	-24.13 \pm 0.19	c
13. $\text{CsUO}_2\text{PO}_4 \cdot 2.5\text{H}_2\text{O}(\text{s}) = \text{Cs}^+ + \text{UO}_2^{2+} + \text{PO}_4^{3-}$	-25.59	c,f	-23.80 \pm 0.20	c

^a At 298 K.

^b This work.

^o Recalculated in this work from reference 14.

^d Recalculated in this work from reference 3.

^c Corrected from $I=0$ to $I=0.23 \text{ mol dm}^{-3}$.

^f Corrected from, $I=0.23 \text{ mol dm}^{-3}$ to $I=0$.

signed on the basis of the procedure published earlier (ref. [5], eqs 1–5). The input data for the program were the concentrations of all components in the solution (table 2) and the values of thermodynamic equilibrium constants at 298 K (table 3, equilibria 1–7). The ionic strength, I , defined as $I=0.5 \sum cz^2$ (c and z are the concentration and valence charge of the ion, respectively) was calculated by an iterative procedure (iterations until the change was less than $\pm 1\%$). Consequently, the values of the equilibrium constants at $I=0$ were calculated from thermodynamic equilibrium constants by using the values of the activity coefficients (γ) of the ions at corresponding ionic strengths. Activity coefficients (at 298 K) of all ions (except UO_2^{2+}) were calculated by using the Davies equation [26]: $\log \gamma = -0.509z^2[\sqrt{I}/(\sqrt{I}+1) - 0.2I]$. For uranyl(2+) ions the activity coefficients determined by Brusilovsky [27] were used. In figure 2 is presented the dependence of the activity coefficients on the ionic strength: for the ions with valence charge 2 the curve was calculated by using the Davies equation (curve 1) and for the uranyl(2+) ions it was constructed by using the experimental values [27] (curve 2). The difference between these two curves is considerable.

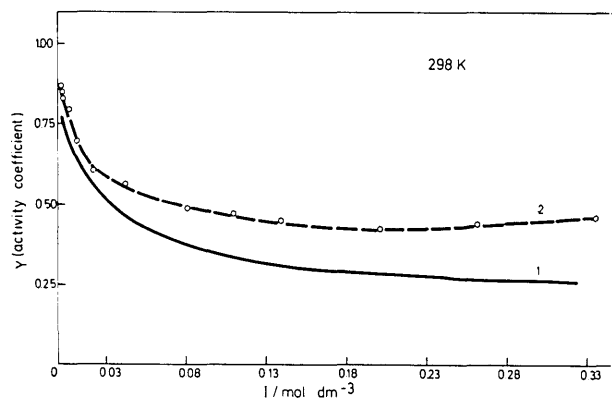


Figure 2. Calculated activity coefficients [26] for the ions with ± 2 valence charge (curve 1) and experimentally determined activity coefficients for UO_2^{2+} [27] (curve 2) as a function of the ionic strength.

The calculated values of the solubility products ($\log K_s$) at the corresponding ionic strengths and the thermodynamic values [$\log K_s (I=0)$] are presented in table 2; $\log K_s (I=0)$ has at 298 K an average value of -26.50 ± 0.09 (table 3, equilibrium 9).

Discussion

Ammonium uranyl(2+)phosphate trihydrate precipitates as the only solid phase in a broad concentration range of the reactants (fig. 1). On the contrary, in the presence of alkali ions, mixtures consisting of hydrogen and alkali uranyl(2+)phosphates prevail [3,4]. These results can be explained by the greater sorption affinity of NH_4^+ on uranylhydrogen(2+)phosphate tetrahydrate as compared to that of alkali cations [28].

In order to compare the solubilities of ammonium and alkali uranyl(2+)phosphates we recalculated the solubility data of Vesely, Pekarek, and Abbrent [14] (experiments performed at $I=0.23 \text{ mol dm}^{-3}$) by using reported association constants of phosphoric acid [23–25] (table 3, equilibria 1–3) and stability constants of uranyl(2+)phosphate complexes [5] (table 3, equilibria 4–7) corrected from $I=0$ to $I=0.23 \text{ mol dm}^{-3}$ (by using experimental activity coefficients of UO_2^{2+} ions [27]). The average values of ionic activity and concentration products are listed (table 3, equilibria 9–13). The solubilities of different uranyl phosphate compounds depend on the cationic species in the structure. The ionic product constants (K_s) increase as follows: $K_s(\text{NH}_4) < K_s(\text{Rb}) < K_s(\text{K}) < K_s(\text{Cs}) < K_s(\text{Na})$.

Our experimentally determined $K_s(I=0)$ values of $\text{NH}_4\text{UO}_2\text{PO}_4 \cdot 3\text{H}_2\text{O}$ and $\text{KUO}_2\text{PO}_4 \cdot 3\text{H}_2\text{O}$ [3] (table 3, equilibria 9 and 11) corrected to $I=0.23 \text{ mol dm}^{-3}$ shows an excellent agreement with the corresponding values recalculated from the data [14] originally determined at $I=0.23 \text{ mol dm}^{-3}$. This confirms the accuracy of the stability constants of the uranyl phosphate complex species [5] and the experimental precision of the solubility data [3,14]. The K_s values determined and those recalculated in this work are in disagreement with the values given by Klygin et al. [13] and Muraveva et al. [29]. These authors did not consider the uranyl(2+)phosphate complex formation. The value of K_s for $\text{KUO}_2\text{PO}_4 \cdot 3\text{H}_2\text{O}$ determined by Chukhlantsev and Stepanov [12] is a hundred times higher than ours, but their solubility product constant of $\text{NH}_4\text{UO}_2\text{PO}_4 \cdot 3\text{H}_2\text{O}$ (at undefined ionic strength) is similar, ($\log K_s = -26.36$) [12], to the value determined in this work (at $I=0$). It seems that (a) experimental uncertainties and (b) calculations which do not take into account complex species compensate each other, giving a value of K_s for $\text{NH}_4\text{UO}_2\text{PO}_4 \cdot 3\text{H}_2\text{O}$ similar to the one we determined. Recalculation of their data [12] is not

possible because the analyses of the equilibrated solutions were incomplete.

The x-ray powder pattern of $\text{NH}_4[\text{UO}_2\text{PO}_4]\cdot 3\text{H}_2\text{O}$ reveals a close structural relationship with the series $\text{M}[\text{UO}_2\text{PO}_4]\cdot n\text{H}_2\text{O}$ ($n=4$ for $\text{M}=\text{Li}$; $n=3$ for $\text{M}=\text{H}_3\text{O}$, Na , K , Rb ; and $n=2.5$ for $\text{M}=\text{Cs}$). The crystal structure of $\text{M}[\text{UO}_2\text{PO}_4]\cdot n\text{H}_2\text{O}$ (fig. 3, structure of $\text{H}_3\text{O}[\text{UO}_2\text{PO}_4]\cdot 3\text{H}_2\text{O}$ [15]) reveals packing arrangements of infinite layers of octahedra and tetrahedra and water layers containing M (H_3O^+ , alkali or NH_4^+) ions. Uranium exhibits an octahedral coordination. The PO_4 tetrahedron acts as a monodentate bridging group; each PO_4 group is coordinated to four UO_2^{2+} ions. A striking structural feature is the arrangement of the water molecules. The size of the hydrogen, alkali and ammonium ionic species in particular compounds affects the content of the crystalline water in the unit-cell.

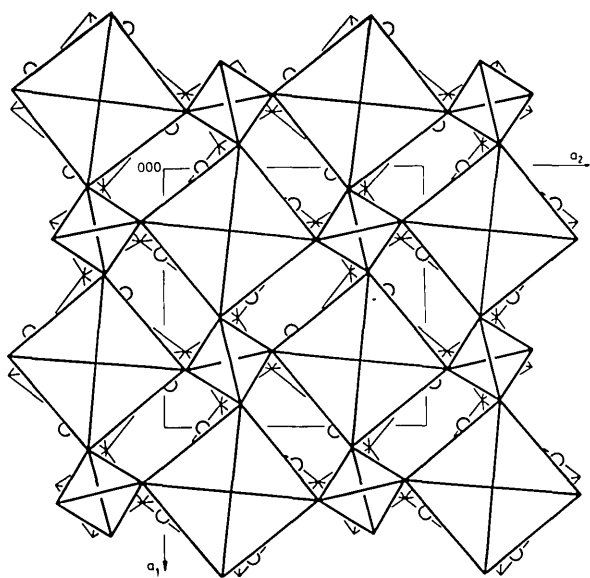


Figure 3. The infinite layers of $[\text{UO}_2\text{PO}_4]^-$ (composed of octahedra and tetrahedra) and water layers in the structure of $\text{H}_3\text{O}[\text{UO}_2\text{PO}_4]\cdot 3\text{H}_2\text{O}$ [15]. The water molecules in the water layer are designated by the open circles.

The unit-cell parameters of alkali uranyl(2+)phosphates are calculated [21,22] from our previously published XRD data [4] and are compared with those of $\text{NH}_4[\text{UO}_2\text{PO}_4]\cdot 3\text{H}_2\text{O}$ (table 4). Calculated unit-cell dimensions of these compounds are in very good agreement with the values obtained from single-crystal data [30]. The increasing values of the unit-cell volumes of the trihydrates $\text{M}[\text{UO}_2\text{PO}_4]\cdot 3\text{H}_2\text{O}$, $\text{M}=\text{Na}$, K , NH_4 , Rb

(table 4), correlate with increasing ionic radii [31] of corresponding species: $\text{Na}(r_1=0.97 \text{ \AA})$, $\text{K}(r_1=1.33 \text{ \AA})$, $\text{NH}_4(r_1=1.43 \text{ \AA})$, and $\text{Rb}(r_1=1.47 \text{ \AA})$.

Table 4. Unit-cell parameters (space group $P4/ncc$, $Z=4$) of hydrogen, ammonium and alkali uranyl(2+) phosphates

Compound	$a/\text{\AA}$	$c/\text{\AA}$	$V/\text{\AA}^3$
$\text{H}_3\text{O}[\text{UO}_2\text{PO}_4]\cdot 3\text{H}_2\text{O}$ [15]	6.995	17.491	855.84
$\text{Li}[\text{UO}_2\text{PO}_4]\cdot 4\text{H}_2\text{O}$	7.04(2)	18.28(7)	906.0
$\text{Na}[\text{UO}_2\text{PO}_4]\cdot 3\text{H}_2\text{O}$	7.01(2)	17.52(4)	860.9
$\text{K}[\text{UO}_2\text{PO}_4]\cdot 3\text{H}_2\text{O}$	7.01(1)	17.84(6)	876.7
$\text{NH}_4[\text{UO}_2\text{PO}_4]\cdot 3\text{H}_2\text{O}$	7.02(1)	18.08(4)	891.0
$\text{Rb}[\text{UO}_2\text{PO}_4]\cdot 3\text{H}_2\text{O}$	7.00(1)	18.36(5)	899.6
$\text{Cs}[\text{UO}_2\text{PO}_4]\cdot 2.5\text{H}_2\text{O}^a$	7.06(2)	17.80(8)	887.2

^a Pseudo tetragonal (monoclinic) [4,30].

The results of this work along with the recalculations of previously published experimental results [3,4,14] give a detailed and complete description of the formation, solubility and structural relationship of ammonium and alkali uranyl(2+) phosphates.

Acknowledgment

The authors express their gratitude to Dr. B. Kojić-Prodić ("Rudjer Bošković" Institute, Zagreb) for fruitful discussion and help during the work. The authors also wish to thank Dr. W. E. Brown (ADAHF Paffenbarger Research Center, NBS) and Dr. W. Wong-Ng (Ceramics Division, NBS) for their suggestions during the final revision of this paper. This work was supported in part by the Self-Management Council for Scientific Research of S. R. Croatia, Yugoslavia, and by the National Bureau of Standards, Gaithersburg, MD (Project No. PP-776, NBS/G-39). One of the authors (M. Marković) was on a Fulbright Scholarship at the ADAHF Paffenbarger Research Center, NBS, where this paper was finalized.

About the authors: Milenko Marković is a research associate presently at the ADAHF Paffenbarger Research Center, NBS, on leave from the Department of Physical Chemistry, "Rudjer Bošković" Institute, Zagreb, Yugoslavia. Nevenka Pavković is an Associate Professor of Physical Chemistry, Faculty of Science, University of Zagreb. Neven D. Pavković, a mechanical engineer experienced in computer science, is employed at the "Rade Končar" Electromechanical Selfmanagement Corporation, Zagreb, Yugoslavia.

References

- [1] Pavković, N., Branica, M., and Težak, B., *Croat. Chem. Acta* **40**, 117 (1968).
- [2] Pavković, N., and Marković, M., *Radiochim. Acta* **34**, 127 (1983).
- [3] Pavković, N., Marković, M., and Kojić-Prodić, B., *Croat. Chem. Acta* **55**, 393 (1982).
- [4] Pavković, N., Marković, M., and Kojić-Prodić, B., *Croat. Chem. Acta* **55**, 405 (1982).
- [5] Marković, M., and Pavković, N., *Inorg. Chem.* **22**, 978 (1983).
- [6] *Proc. Low-Grade Uranium Ores*, I.A.E.A., Vienna, 1967.
- [7] Harrington, D. C., and Ruehle, A. E., *Uranium Production Technology*, Van Nostrand, New York, 1959.
- [8] Linstead, R. P., Burstall, F. M., and Arden, T. V., *British Patent* 759900, 1956.
- [9] Von Huber, H., *Atomwirtschaft-Atomtechn.* **20**, 127 (1976).
- [10] *Powder Diffraction File: Inorganic Phases*, Joint Committee on Powder Diffraction Standards, Swarthmore, 1986.
- [11] Weigel, F., and Hoffman, J., *J. Less-Common Met.* **44**, 99 (1976).
- [12] Chukhlantsev, V. G., and Stepanov, S. I., *Zh. Neorg. Khim.* **1**, 478 (1956).
- [13] Klygin, A. E., Zabraznova, D. M., and Nikolskaya, N. A., *Zh. Anal. Khim.* **16**, 297 (1961).
- [14] Vesely, V., Pekarek, V., and Abbrent, M., *J. Inorg. Nucl. Chem.* **27**, 1159 (1965).
- [15] Morosin, B., *Acta Cryst.* **B34**, 3732 (1978).
- [16] Wilson, C. L., and Wilson, D. W., *Comprehensive Analytical Chemistry*, Vol. Ic, Elsevier, Amsterdam, 1962, p. 611.
- [17] Vogel, A. I., *A Textbook of Quantitative Inorganic Analysis*, 2nd ed., Longmans, Green and Co., London, 1951, p. 245.
- [18] *Analiticheskaya Khimiya Elementov-Uran*, Akad. Nauk SSSR, Moscow, 1962, p. 62.
- [19] *Vogel's Textbook of Quantitative Inorganic Analysis*, 4th ed., Longmans, Green and Co., New York, 1978, pp. 499, 756, 837.
- [20] Kobets, L. V., Kolevich, T. A., and Umreiko, D. S., *Zh. Neorg. Khim.* **23**, 909 (1978).
- [21] Popović, S., and Kojić-Prodić, B., *Fizika* **12**, 329 (1980).
- [22] Appleman, D. E., and Evans, Jr., H. T., Report PB 216188, 1973, U.S. Dept. of Commerce, National Technical Information Service, Springfield.
- [23] Bates, R. G., *J. Res. Natl. Bur. Stand. (U.S.)* **47**, 127 (1951).
- [24] Smith, R. M., and Martell, A. E., *Critical Stability Constants*, Vol. 4, Plenum Press, New York, 1976.
- [25] Ender, F., Teltshik, W., and Schäfer, K., *Z. Elektrochem.* **61**, 775 (1957).
- [26] Stumm, W., and Morgan, J. J., *Aquatic Chemistry*, 2nd ed., Wiley-Interscience, New York, 1981, p. 135.
- [27] Brusilovsky, S. A., *Dokl. Akad. Nauk SSSR* **120**, 305 (1958).
- [28] Pekarek, V., and Benešova, M., *J. Inorg. Nucl. Chem.* **26**, 1743 (1964).
- [29] Muraveva, I. A., Zaborenko, K. B., Nemkova, O. G., and Khan De Pin, *Radiokhim.* **6**, 124 (1964).
- [30] Schulte, E., *Neues Jahrb. Mineral Monatsch.*, 242 (1965).
- [31] *Handbook of Chemistry and Physics*, 58th ed., Weast, R. C. (editor), CRC, 1977/78.

Practical Uncertainty Limits to the Mass Determination of a Piston-Gage Weight

Volume 93

Number 4

July–August 1988

R. S. Davis and B. E. Welch

National Bureau of Standards
Gaithersburg, MD 20899

The mass of a 590-g piston-gage weight was determined with a standard error of 0.057 mg (0.1 ppm). The sources of error are carefully examined. These include air-buoyancy corrections, physically adsorbed surface moisture, and air-convection within the weighing chamber. We conclude that significant improvement cannot be realized with

the conventional weighing techniques available to most piston-gage users.

Key words: analytical balance; calibration; mass; piston-gage; surface effects; weighing; weighing errors.

Accepted: February 25, 1988

1. Introduction

The equilibrium pressure in a piston gage is related in a fundamental way to the gravitational force on the rotating parts and area of the piston. The gravitational force, in turn, is determined by the product of the local gravitational acceleration and the sum of the masses of each rotating component. When piston gages are operated in the absolute mode, additional forces associated with the atmosphere, such as air buoyancy, are absent. These forces must be considered in gage-mode operation.

In this paper, we will focus on the problem of assigning mass values to piston-gage weights of about 590-g nominal mass. The goal of these measurements is that the uncertainty in the mass calibration lead to an error in the maximum pressure generated by the rotating assembly of less than 1 ppm (1×10^{-6}). This level of accuracy is motivated by research underway at NBS which seeks to achieve unprecedented levels of accuracy in the calibration of selected piston gages. The standard used in these measurements is a mercury manome-

ter which has an error of the order of 1 ppm in the pressure range from 10 to 130 kPa [1].

Most of the rotating mass of a piston gage is in a stack of 590-g weights. The uncertainty of the mass of such a stack of weights is the direct sum of uncertainties systematic to the calibration of each weight, combined with the root-sum-square of the random uncertainty associated with each weight. Thus to achieve the desired total uncertainty, care must be taken in characterizing both types of error. We describe in detail how we have evaluated the total uncertainty of our mass measurements. Particular attention will be paid to errors which are systematic to a given measurement technique and thus difficult to detect. These errors can amount to 1 ppm and are, therefore, important to the end result. By contrast, the NBS mass calibration service typically provides an uncertainty of 0.04 ppm (one standard deviation) for calibrations of a single 500-g standard of the highest commercially-available quality.

2. Assignment of Mass (Ideal)

A mass m_X is assigned to a piston-gage weight by comparison with a known standard of mass m_S . The comparison is done under ambient atmospheric conditions. The following formula is then used to determine m_X [2]:

$$m_X = m_S \cdot (1 - \rho/\rho_S)/(1 - \rho/\rho_X) + \Delta, \quad (1)$$

where

ρ = density of the air within the balance case ($\approx 1.2 \text{ mg/cm}^3$),

ρ_S = density of the standard ($\approx 8 \text{ g/cm}^3$),

ρ_X = density of the piston-gage weight ($\approx 7.8 \text{ g/cm}^3$),

Δ = difference between balance readings corresponding to S and X ($-2 \text{ mg} < \Delta < 2 \text{ mg}$).

We can estimate the expected uncertainty in m_X by simple propagation of error through eq (1). The standard S is calibrated in SI units of mass with an uncertainty of about 0.04 ppm. (In this paper, we will use the BIPM recommendation for combining errors. All uncertainties are given as estimates of one standard deviation.) This uncertainty propagates directly as a 0.04 ppm uncertainty in m_X . The air density ρ becomes increasingly important as the density of X diverges from that of S. In the present situation, the two densities are nearly equal. Therefore, a measurement of ρ to a modest 1 percent will propagate as an error of less than 0.04 ppm in m_X . The air density ρ is determined from measurements of barometric pressure, temperature within the balance case, and relative humidity. With these data, ρ can be determined to sufficient accuracy through the use of an equation of state for moist air [3]. The balance used has a precision of 0.040 mg (one standard deviation). By averaging several repeated measurements, the contribution of error in Δ to the final result can be made arbitrarily small, *so long as all errors are randomly distributed*. Most of this article will be devoted to examining the sources and magnitudes of all known errors in Δ .

The contribution of uncertainty in ρ_S and ρ_X to the total error in m_X deserves discussion. Suppose a weight T is calibrated in air of density ρ_1 . Since the calibration is done in air, the mass value m_T assigned to T will depend on the density ρ'_T which is assigned to the weight. Now suppose that the actual density of T is ρ_T ; whenever T is used as a standard in subsequent mass or force measurements, use of the assigned mass value m_T and the

assumed density ρ'_T will produce an error whose magnitude is

$$E = |(\rho_1 - \rho_2)(1/\rho'_T - 1/\rho_T)|, \quad (2)$$

where ρ_2 is the air density during the subsequent measurement. From eq (2) it is clear that the error E will be small if $\rho_1 \approx \rho_2$. This is always true for the standard S, which is always used at normal laboratory conditions. Thus the density of S need only be known to an uncertainty of about 1 percent and a value of density obtained from a metals handbook will suffice. The piston-gage weight X, however, will sometimes be used in vacuum ($\rho_2 \approx 0$). In order that E be less than 0.05 ppm when the piston-gage is operated in the absolute mode, ρ_X must be uncertain to no more than 0.03 percent. To achieve the needed accuracy, the densities of the piston-gage weights were measured by hydrostatic weighing.

3. Known Problems

When using a conventional commercial balance, eq (1) may be considered an accurate mathematical model to a level of about 0.5 ppm (0.3 mg for a 590-g weight). In particular, errors in Δ can usually be considered random at this level. Averaging of repeated measurements of Δ may produce a more accurate value below 0.5 ppm, but this assumption must be tested. The problems indicated in sections 3.1–3.5 may occur.

3.1 Between-Times Error

Identical series of measurements taken on different days may differ by significantly more than the combined random uncertainties of each day. The additional uncertainty may itself be randomly distributed, however. If this is so, it is referred to as a “between-times” error (with a characteristic standard deviation σ_b) to distinguish it from the random error observed within a single series of measurements (with a characteristic standard deviation σ_w) [4]. The presence of a significant between-times component of error is usually unforeseen and its source impossible to determine. The total random error σ_t in the average of a series of duplicated measurements will be:

$$\left(\frac{\sigma_b^2}{m} + \frac{\sigma_w^2}{nm} \right)^{1/2},$$

where n is the number of repeated measurements within each run and m is the number of runs on

separate days. If only one day's measurements are used, then $m = 1$. In this case, it is clear that by increasing n one will arrive at a point where the total error is dominated by σ_b . At this point, increasing n further is wasted effort. It is usual to assume that σ_b is negligible. This assumption should be checked, especially when using a new measurement system or when relying on statistical averaging to reduce uncertainties by a factor of three or more.

3.2 Surface Moisture

The surface of stainless steel in air is covered with moisture. At room temperature, the mass per unit area of this moisture layer will depend on the relative humidity and the surface finish of the alloy. Kochsiek has found that metals generally have 0.1 to 0.3 $\mu\text{g}/\text{cm}^2$ of adsorbed moisture at 50 percent relative humidity and at room temperature [5]. His studies were done gravimetrically. Yoshimori et al. used chemical analysis to determine the moisture given up by metals into a pure argon atmosphere as a function of temperature [6]. The lowest temperature studied was 100 °C. Thus their results represent an upper limit to the moisture which would be given up at room temperature. This being the case, their results are consistent with those of Kochsiek. Thus weights calibrated at laboratory conditions and which have surface area and finish different from the standard will have a mass which, at some level, will depend on the ambient relative humidity. The magnitude of this effect is difficult to calculate quantitatively but should appear as a correlation of the calibration results with relative humidity.

When the calibrated weight is then used in a vacuum (relative humidity of zero) its mass will be lower to the extent that adsorbed moisture is removed. Based on [4] and [5], this effect may be negligible or it may be as great as 0.2 ppm in the mass of a piston-gage weight. A definitive answer to this question is beyond the scope of the present study.

3.3 Weight Stability

The question of surface moisture can be thought of as one aspect of weight stability. The best-quality commercial weights have physical characteristics which conform to ASTM Type 1 Grade S [7]. A weight with no sharp edges and made of a single-piece of non-magnetic stainless steel conforms to these specifications so long as its surface has the

following properties: 1. Area does not exceed twice the area of a cylinder of equal height and diameter; 2. Highly polished except for markings and adjustment area, free of pits and pores. According to the first surface requirement, the surface area of a 590-g weight may not exceed 200 cm^2 . As can be seen in table 1, the piston-gage weight fails to meet this specification. As for the second requirement, our piston-gage weights are free from pits and pores but are not polished. Thus the piston-gage weights may not be as stable as the best quality laboratory weights.

Table 1. Pertinent physical characteristics of the weights designated X and T in the text

	X	T
Nominal mass (g)	590	590
Density at 20 °C ($\text{kg}\cdot\text{m}^{-3}$)	7837	7868
O.D. (mm)	135	75
I.D. (mm)	70	n.a.
Thickness (mm)	7	17
Surface area (cm^2)	250	130

3.4 Gravitational Gradient

Weighing with an analytical balance relies on the existence of a local, constant, gravitational acceleration. The actual value of this acceleration cancels out of eq (1). Cancellation will not be perfect, however, if the centers of mass of the standard and unknown are placed on the balance at different elevations with respect to the earth. The lack of cancellation is due to the gravitational gradient at the earth's surface (about -0.003 ppm/cm [8]). If left uncorrected, the gravitational gradient would produce only a small systematic error.

3.5 Lack of Thermal Equilibrium

Equation (1) assumes that both the standard and unknown are in thermal equilibrium with the air in the balance chamber. Violation of this condition may produce non-negligible systematic errors in the results.

These errors are presumably due to forces caused by motion of the air in the balance case driven by thermal gradients. Two types of thermal problems may be distinguished. The first, which has received considerable recent study by Schoonover and Taylor [9], arises when the standard or the unknown is maintained at a different temperature from the balance chamber itself. If

both standard and unknown are maintained at the same temperature offset from the balance temperature, errors may still be negligible provided the two objects have identical geometry.

A second thermal problem may arise from a heat source at some point around the balance case. The balance operator may be one such heat source. This effect is more difficult to study and has not received much recent attention in analytical weighing. Schürmann et al. produced a theory which applies to these types of forces and tested it with a series of experiments [10]. In one experiment, however, the observed force due to air convection was 40 times greater than the prediction. Some cancellation of unwanted effects should also be seen for this type of thermal problem if the standard and unknown have identical geometries.

4. Design of Calibration

Confronted with the need to calibrate a set of 590-g piston-gage weights to better than 1 ppm and faced with the set of known or suspected problems listed in the previous section, we designed the following measurement system. Weighings were carried out on a H315-MC Mettler balance¹. This is a single-pan mechanical balance with 1-kg capacity. We will refer to this balance as Bal-2. The balance was housed in a double-walled aluminum box with foam insulation between the walls. Standards and unknowns could both be stored inside the box. A small door in front of the box allows the operator to move objects manually on and off the balance pan. A small window allows the operator to observe the balance chamber and the scale reading. The balance arrestment mechanism is fed through the outer box and thus can be manipulated remotely by the operator.

Each piston-gage weight (X) is approximately washer-shaped. Pertinent physical properties are shown in table 1. The outer diameter of each weight is too large to permit it to lie flat on the balance pan. Instead, it is hung from a hook centered between the two vertical pan supports. The hook is at sufficient height so that the suspended weight clears the pan. Based on considerations in section 3, minimum errors should be obtained

when weighing by double substitution [11] against a standard of similar geometry which is also suspended from the same hook. Thus one of the piston-gage weights (X1, say) should serve as the standard for calibrating the remaining weights. The problem then reduces to calibrating X1 the best way possible.

The best balance available to us was the NBS primary kilogram comparator (Bal-1). This operates at a fixed load of 1-kg and has a precision of 1.5 μg (one standard deviation) for a single observation. Of equal importance, all manipulations are automated and carried out by remote control. Thus temperature gradients within the balance chamber do not exceed 5 mK side-to-side. A vertical temperature gradient of about +0.5 mK/cm is imposed for stability [12].

There is, unfortunately, no way in which X1 can be calibrated directly on this balance. Instead, we constructed a transfer standard (T) whose physical properties are also given in table 1. The virtue of T is that it can be calibrated using the kilogram comparator and then used to calibrate X1. When being calibrated, it lies flat with an additional 410 g of calibrated standards placed on top. When used to calibrate X1, T can be suspended from the hook. A hole 1 cm in diameter is drilled through T for this purpose. The placement of the hole was determined by constraining the center-of-mass of T to have the same elevation as that of X1 when suspended from the same hook. When compared on Bal-2, the two weights T and X1 are stored outside the balance (but within the insulated box) hanging side-by-side on hooks at the same elevation as the hook within the balance. The weights were always allowed to equilibrate overnight before measurements were begun.

As a check on the measurement scheme, we also calibrated X1 and T directly against the same set of standards using Bal-2. Both X1 and T were hung from the hook and stored outside the balance as described above. The collection of standard weights was stored inside the box on an aluminum plate at the same elevation as the balance pan. While we might expect systematic errors from various sources in each calibration of X1 and T, we do not expect that the difference in mass between X1 and T measured this way should differ significantly from that found from direct intercomparison. The effect of the gravitational gradient on these measurements requires a correction of about 0.015 mg, which was applied in order to obtain the results presented in this paper. As a matter of interest, we repeated the measurement of T against the set of

¹ Brand names are used solely to identify the apparatus used. Such identification neither implies endorsement by the National Bureau of Standards, nor does it imply that the particular product or equipment is necessarily the best available for the purpose.

standards. This time, however, T was placed flat on the balance pan and stored flat on the aluminum plate alongside the standards.

We also measured T and X1 against the same set of standards on a different balance. The balance was another H315-MC located in the NBS mass calibration laboratory (Bal-3). For this balance, the method described by Schoonover and Taylor for minimizing thermal problems is used [8]. In this scheme, there is no box around the balance. Instead, a massive aluminum plate is placed next to the balance. Active servo-control maintains the plate at the same temperature as a probe located at the front of the weighing chamber. Weights placed on the plate are covered with an aluminum can and allowed to equilibrate overnight. The thermal load represented by the operator is simulated by a heating element when the operator is not present. Using this set-up, T and X1 were placed flat on the plate in order to come into thermal equilibrium. During balance observations, T was placed flat on the pan and X1 was tilted so that it was constrained at top and bottom by the two pan supports (i.e., this balance was not equipped with a hook for weighing X1).

5. Results

5.1 Calibration of T (Bal-1)

As mentioned above, T was calibrated using the NBS primary kilogram comparator. We did not have an opportunity to search for a possible between-times component to this calibration. However, such a component is negligible in the comparison of platinum/10 percent iridium and stainless-steel kilograms, which differ markedly in physical properties. The result of the calibration of T is shown in table 2 along with the estimated standard deviation. All known errors reported in this and succeeding tables have been estimated by statistical methods. Errors estimated in this way are sometimes referred to as Type A errors.

Table 2. Mass value and error budget for calibration of T on Bal-1

Mass of T: 590.049 383 g	
Uncertainty:	
	Type A
Reference standards	0.024 mg
Buoyancy correction	nil
Standard deviation	0.002 mg
RSS total	0.024 mg

5.2 Calibration of X1 (Bal-2)

The two weights T and X1 were compared on four different days. The result of each day's comparison was taken as the average of at least four duplicate measurements. No between-times component is discernible within the limited sample of measurements. The standard deviation σ_w of the balance used is taken to be 40 μg . This number is based on a large number of degrees of freedom. Each day's results are considered to be representative of the long-term standard deviation so long as they pass an F-test at the 90 percent level of confidence. The mass value assigned to X1 is based on the measured difference between T and X1 and the assigned mass value of T. Results are summarized in table 3.

Table 3. Mass value and error budget for calibration of X1 on Bal-2

Mass of X1: 590.034 153 g	
Uncertainty:	
	Type A
Reference standard (T)	0.024 mg
Buoyancy correction	
from ρ_a	nil
from ρ_x	0.006 mg
Mean standard deviation	0.012 mg
RSS total	0.027 mg

5.3 Check of Closure (Bal-2)

A set of calibrated standards was used to calibrate X1 and T in separate experiments. Again, no between-times component to the uncertainty was observed. The results are summarized in table 4.

Table 4. Mass values and error budget for calibration of X1 and T with respect to the same standards; measurements on Bal-2

(1) Mass of X1 (hanging):	590.034 232 g
(2) Mass of T (hanging):	590.049 513 g
(3) Mass of T (flat):	590.049 325 g
Uncertainty:	
	Type A
Reference standards	0.022 mg
Buoyancy correction	nil
Mean standard deviation	0.004 mg (1)
	0.018 mg (2), (3)
RSS total	0.022 mg (1)
	0.028 mg (2), (3)

5.4 Check Using Bal-3

The same standards used in the closure check were also used to calibrate T and X1 on Bal-3. In this case, T was measured when placed flat on the pan and X1 was measured as described above in section 5. The results are shown in table 5.

Table 5. Mass values and error budget for calibration of X1 and T with respect to the same standards; measurements on Bal-3

Mass of X1 (tilted):	590.033 986 g
Mass of T (flat):	590.049 424 g
Uncertainty:	
	Type A
Reference standards	0.022 mg
Buoyancy correction	nil
Mean standard deviation	0.016 mg
RSS total	0.027 mg (1)

6. Discussion

There are several striking discrepancies in the results at the level of about 0.3 ppm in the mass of X1 or T. Perhaps the most interesting of these is that, when the same standard weights were used with Bal-2, the mass value computed for T depended on whether T was suspended from the hook or was placed flat on the pan. As seen in table 4, the difference in these two results is 188 μg , more than seven times greater than the combined standard deviation based on the random errors of each measurement. The discrepancy cannot be explained by changes in the ambient relative humidity. We reoriented the hook and repeated the measurements to check whether geometrical imperfections in the balance could be the cause of the discrepancy. The results, however, were the same. The mass obtained when T was flat is consistent with that obtained on Bal-1. The latter measurement is assumed free from significant errors due to lack of thermal equilibrium.

The difference in mass between T and X1 when measured directly (mass of X1 from table 3 subtracted from mass of T from table 2) and when inferred from measurements of each weight against a common set of standards (mass of X1 subtracted from mass of T, both from table 4 in hanging orientation) disagree by 50 μg . This represents 2.8 times the combined standard deviation assigned to the results. Again, differences in the ambient relative humidity cannot reasonably explain the discrepancy. As an indication of our inability to offer

any plausible explanation for this lack of agreement, we will include an additional 50 μg error to the mass value assigned to X1, giving a new total of 0.057 mg (0.1 ppm).

The results obtained on Bal-3 are also interesting. In this case, the value found for the mass of T agrees rather well (1.1 times the combined standard deviations) with the accepted value obtained on Bal-1. The result for X1, however, is significantly lower than the value shown in table 3. It is, perhaps, noteworthy that the discrepancies found on Bal-3 are anticorrelated with those obtained from similar measurements on Bal-2. In fact the average of the discrepant measurements taken on Bal-2 and Bal-3 (that is, direct calibrations of T and X1 against the same set of standards) agrees well with the values shown in tables 2 and 3. In retrospect, it would have been interesting to attempt these measurements on Bal-2 or Bal-3 with no auxiliary apparatus to bring the weights into good thermal equilibrium with the balance chamber—this is the condition in most laboratories and, we suspect, might lead to even larger errors than those we encountered.

Finally, we wish to emphasize that the observed discrepancies cannot be explained by errors in the correction due to air buoyancy [eq (1)], as a calculation will now show. If the air density within the weighing chamber has a significant vertical gradient, then eq (1) must be modified:

$$m_X = m_S \cdot (1 - \rho_L / \rho_S) / (1 - \rho_U / \rho_X) + \Delta. \quad (1a)$$

In eq (1a), ρ_L is the mean air density in the vicinity of the standards which are placed on the pan in the lower part of the balance chamber. Similarly, ρ_U is the mean air density in the vicinity of T when it is hanging from the hook near the top of the balance chamber. If one were mistakenly to assume that $\rho_U = \rho_L$, then m_X would be overestimated by approximately

$$m_S(\rho_L - \rho_U) / \rho_X.$$

In order to account for the observed discrepancies found when Bal-2 was used to measure T flat on the pan and suspended from the hook, there would need to be a difference in air density of about 0.2 percent from the pan to a point about 9 cm above the pan. This translates to a gradient in pressure of 22 Pa/cm or a temperature gradient of 70 mK/cm. Both these numbers are unrealistically large.

7. Conclusions

We believe that the mass assigned to X1 in table 3 has a total uncertainty of 0.057 mg and that this uncertainty approaches the best results which can be achieved by conventional weighing techniques using a commercial analytical balance. There is some indication that, even when thermal problems of the type examined by Schoonover and Taylor have been overcome, other problems remain. Perhaps the origin of these additional problems can be found in the model of Schürmann et al. In addition, we have pointed to questions concerning changes in the mass of piston-gage weights between atmospheric and vacuum conditions due to loss of surface moisture. This uncertainty is of equal magnitude to the present uncertainty of the mass of these weights as determined from weighing in air. We have not studied questions of routine cleaning and handling of piston-gage weights, although such questions may be pertinent.

Improvement in the assignment of mass to piston-gage weights used in the absolute mode would require two innovations. First, the weights themselves must be reduced in surface area as much as possible. Since the shape of the weights cannot practically be changed, the only improvement possible is to polish the weights to a specular finish. Second, the mass of weights should, ideally, be determined in vacuo. Since mass standards are themselves calibrated in air, use of mass standards in vacuo to calibrate a piston-gage weight would require additional surface studies. Vacuum weighing, on the other hand, offers the simplification that buoyancy corrections and air convection are negligible. This advantage may prove to be overwhelming if improved accuracy is required.

8. Acknowledgments

We are pleased to acknowledge the assistance of several colleagues. Randall Schoonover designed the enclosure for Bal-2 and offered many useful suggestions. Walter Markus constructed the enclosure for Bal-2. James Taylor wrote the computer program used to analyze much of our data. Jerry Keller calibrated the auxiliary mass standards used in this work.

About the authors: R. S. Davis is a physicist in the Length and Mass Division of the NBS Center for Basic Standards and B. E. Welch is a physicist in the Temperature and Pressure Division of the NBS Center for Basic Standards.

References

- [1] Guildner, L. A., Stimson, H. F., Edsinger, R. E., Anderson, R. L., An Accurate Mercury Manometer for the NBS Gas Thermometer. *Metrologia* **6**, 1 (1970).
- [2] Heydemann, P. L. M., and Welch, B. E., Piston Gages, chapter 4, in *Experimental Thermodynamics on Non-reacting Fluids*, LeNeidre, B., and Vodar, B., eds., Butterworths, London (1975) pp. 147–202.
- [3] Jones, Frank E., The Air Density Equation and the Transfer of the Mass Unit. *J. Res. Natl. Bur. Stand. (U.S.)* **83**, 419 (1978). (The simplified formula given in eqs (44) and (45) suffices for the work reported here.)
- [4] Croarkin, C., Measurement Assurance Programs Part II: Development and Implementation, *Natl. Bur. Stand. U.S. Spec. Publ. 676II* (April 1985).
- [5] Kochsiek, M., Measurement of Water Adsorption Layers on Metal Surfaces. *Metrologia* **18**, 153 (1982).
- [6] Yoshimori, T., Ishiwari, S., Watanabe, Y., Harada, T., and Yamada, S., Coulometric Microdetermination of Glasses and of Hydrogen in Beryllium Metal. *Trans. Japan. Inst. Met.* **14**, 396 (1973).
- [7] ASTM E617-81. Standard Specifications for Laboratory Weights and Precision Mass Standards. 1986 Annual Book of ASTM Standards **14.02**, 480–499.
- [8] For instance, Almer, H. E., and Swift, H. F., Gravitational Configuration Effect upon Precision Mass Measurements. *Rev. Sci. Instrum.* **46**, 1174 (1975).
- [9] Schoonover, R. M., and Taylor, J. E., Some Recent Developments at NBS in Mass Measurements. *IEEE Trans. Instrum. Meas.* **IM-35**, 418–422 (1986).
- [10] Schürmann, J. W., Massen, C. H., and Poulis, J. A. The Influence of Free Gas Convection on Balance Readings. Gast, Th. and Robens, E., eds., *Progress in Microbalance Techniques Vol. I*, Heyden and Son Ltd., London (1972) pp. 189–196.
- [11] Jaeger, K. B., and Davis, R. S., A Primer for Mass Metrology. *Natl. Bur. Stand. (U.S.) Spec. Publ. 700-1* (November 1984).
- [12] Macurdy, L. B., Response of Highly Precise Balances to Thermal Gradients. *J. Res. Natl. Bur. Stand. (U.S.)* **68C**, 135 (1964).